



CERN-EP-2016-278
4 November 2016

W and Z boson production in p–Pb collisions at $\sqrt{s_{\text{NN}}} = 5.02$ TeV

ALICE Collaboration*

Abstract

The W and Z boson production was measured via the muonic decay channel in proton–lead collisions at $\sqrt{s_{\text{NN}}} = 5.02$ TeV at the Large Hadron Collider with the ALICE detector. The measurement covers backward ($-4.46 < y_{\text{cms}} < -2.96$) and forward ($2.03 < y_{\text{cms}} < 3.53$) rapidity regions, corresponding to Pb-going and p-going directions, respectively. The Z-boson production cross section, with dimuon invariant mass of $60 < m_{\mu\mu} < 120$ GeV/ c^2 and muon transverse momentum (p_{T}^{μ}) larger than 20 GeV/ c , is measured. The production cross section and charge asymmetry of muons from W-boson decays with $p_{\text{T}}^{\mu} > 10$ GeV/ c are determined. The results are compared to theoretical calculations both with and without including the nuclear modification of the parton distribution functions. The W-boson production is also studied as a function of the collision centrality: the cross section of muons from W-boson decays is found to scale with the average number of binary nucleon-nucleon collisions within uncertainties.

arXiv:1611.03002v2 [nucl-ex] 2 Apr 2017

© 2016 CERN for the benefit of the ALICE Collaboration.

Reproduction of this article or parts of it is allowed as specified in the CC-BY-4.0 license.

*See Appendix A for the list of collaboration members

1 Introduction

The W and Z boson production is extensively studied at hadron colliders as it represents an important benchmark of the Standard Model. The measurements in pp and p \bar{p} collisions at different energies [1–13] are well described by Quantum Chromodynamics (QCD) calculations at Next-to-Leading Order (NLO) and Next-to-Next-to-Leading Order (NNLO) in perturbation theory. In the calculations, the input electroweak parameters (e.g. boson masses and weak couplings) are known to high accuracy, as well as the radiative corrections [14]. The measurements can hence constrain the Parton Distribution Functions (PDFs) [15].

With the large centre-of-mass energies and luminosity of the Large Hadron Collider (LHC), the W and Z boson production has become accessible for the first time in proton-nucleus [16–19] and nucleus-nucleus collisions [20–23]. The PDFs are expected to be modified for nucleons inside a nucleus compared to those of nucleons in vacuum. Nuclear PDFs (nPDFs) are extracted from global analyses performed at NLO accuracy in perturbative QCD [24, 25], but the results are mostly constrained by Deep-Inelastic Scattering and Drell-Yan data in a limited region of the four-momentum transfer Q^2 and parton longitudinal momentum fraction Bjorken- x [25]. The W and Z bosons and their lepton decay products are unaffected by the hot and dense strongly-interacting matter formed in ultra-relativistic heavy-ion collisions and offer a unique opportunity to study the nPDF in a region of high $Q^2 \sim (100 \text{ GeV})^2$ and Bjorken- x ranges from $\sim 10^{-4}$ to almost unity where they are poorly constrained by data [26]. Furthermore, the asymmetry in the production of positive and negative W bosons, occurring mainly in the processes $u\bar{d} \rightarrow W^+$ and $d\bar{u} \rightarrow W^-$ at the LHC energies, can be used to probe the flavour modification of the quark densities in nuclei [26].

The W and Z boson production was measured in Pb–Pb collisions at $\sqrt{s_{\text{NN}}} = 2.76$ TeV by the ATLAS [20, 21] and the CMS [22, 23] experiments in the electronic and muonic decay channels. The results confirm that the production cross section scales with the number of nucleon-nucleon collisions (binary scaling) within uncertainties on the order of 10%. The W and Z bosons were further studied in p–Pb collisions at $\sqrt{s_{\text{NN}}} = 5.02$ TeV. The Z-boson production was measured by the ATLAS [16] and CMS [17] experiments at mid-rapidity in the leptonic decay channels, and by the LHCb experiment at forward rapidities [18] in the muonic decay channel. The W-boson production was measured by the CMS experiment at mid-rapidity [19] in the leptonic (e, μ) decay channel. The results are described by theoretical calculations both with and without including the nuclear modification of the PDFs, with a preference towards the former and can be used to further constrain the nPDFs [26].

In nucleus-nucleus collisions, particle production is often studied as a function of the collision centrality, which is directly related to the impact parameter of the collision. The number of interacting nucleons, and hence the energy deposited in the collision region, increases from peripheral to central (head-on) collisions thus affecting the volume and density of the strongly-interacting medium that is produced. The nuclear modification of the PDFs is expected to depend as well on the position of the nucleon inside the nucleus, and therefore on average on the impact parameter of the collision [27]. The centrality of nucleus-nucleus collisions is usually estimated by measuring either the energy deposition or the hadronic multiplicity in specific detectors. This estimation is known to be biased in p–Pb collisions, where the range of the multiplicity is of similar magnitude as its fluctuations [28]. The biases are minimised when the centrality is determined through the energy measured at beam rapidity (with zero degree calorimeters), which is deposited by the non-interacting (spectator) nucleons emitted from the Pb nucleus in the collision and is therefore independent of the fluctuations in the number of produced particles.

The W and Z boson production occurs in hard scattering processes at the initial stage of the collision, and it is expected to scale with the number of binary nucleon-nucleon collisions. The centrality-dependent yield can be therefore used as a test bench for the centrality estimation at the LHC.

In this article, the ALICE results on Z and W boson production in the muonic decay channel in p–Pb

collisions at $\sqrt{s_{\text{NN}}} = 5.02$ TeV are presented. The former is measured with smaller uncertainties than the corresponding LHCb measurement in a similar rapidity range. The latter is the first measurement of W production in p–Pb collisions at forward and backward rapidity, in a region that is complementary to the one explored by CMS. The article is organized as follows. The data sample and analysis strategies are described in Section 2. The results are shown in Section 3 and summarised in Section 4.

2 Data analysis

2.1 Experimental apparatus and data samples

The ALICE detector is described in detail in [29]. Muons are reconstructed in the muon spectrometer, covering the pseudorapidity range $-4 < \eta < -2.5$ in the laboratory frame. The spectrometer consists of a dipole magnet with a 3 Tm integrated magnetic field, five tracking stations made of Multi-Wire Proportional Chambers with Cathode Pad readout, and two trigger stations made of Resistive Plate Chambers and several absorption elements. The tracking stations are placed downstream from a conical front absorber made of carbon, concrete and steel, with a thickness of 4.1 m (corresponding to 10 nuclear interaction lengths, λ_I) that filters out hadrons from the interaction point. The trigger stations are placed after an iron wall with a thickness of 1.2 m ($7.2 \lambda_I$) that absorbs secondary hadrons escaping from the front absorber and low-momentum muons, mainly coming from the decay of light hadrons. Finally, a conical beam shield covering the beam pipe protects the spectrometer from particles produced in the interaction of large- η particles with the pipe itself.

In this analysis, the position of the interaction vertex is measured with the Silicon Pixel Detector (SPD), which constitutes the two innermost layers of the Inner Tracking System, covering an acceptance interval of $|\eta| < 2$ and $|\eta| < 1.4$, for the first and second layer, respectively. Two arrays of scintillators, the V0 detector [30], placed on each side of the interaction point and covering the pseudrapidity regions $2.8 < \eta < 5.1$ and $-3.7 < \eta < -1.7$, are used as trigger detectors and to reject beam-induced background. The V0 is also used as a luminometer, together with the T0 detector, which consists of two arrays of quartz Cherenkov counters covering the pseudrapidity regions $4.6 < \eta < 4.9$ and $-3.3 < \eta < -3.0$. The neutron zero degree calorimeters (ZN), placed on either side of the interaction point at ± 112.5 m along the beam pipe are used to estimate the centrality of the collision.

The analysis is performed on data collected in 2013 in proton–lead collisions at a centre-of-mass energy $\sqrt{s_{\text{NN}}} = 5.02$ TeV. Due to the different energies of the proton and lead beams ($E_p = 4$ TeV and $E_{\text{Pb}} = 1.58$ TeV per nucleon), the resulting nucleon–nucleon centre-of-mass is boosted with respect to the laboratory frame by $\Delta y = 0.465$ in the direction of the protons. Data were collected in two configurations, by inverting the direction of the p and Pb beams. It is assumed that the proton beam travels towards positive rapidities. With this convention, muons are measured at forward rapidity ($2.03 < y_{\text{cms}} < 3.53$) when the proton travels towards the spectrometer and at backward rapidity ($-4.46 < y_{\text{cms}} < -2.96$) when the Pb ion is travelling towards the spectrometer. In the following, the two configurations will be referred to as p-going and Pb-going directions, respectively.

The data sample used in the W-boson analysis consists of events with at least one muon candidate track selected with the muon trigger with a transverse momentum $p_T \gtrsim 4.2$ GeV/c, in coincidence with a Minimum Bias (MB) event, which is defined by requiring the coincidence of signals in the two arrays of the V0 detector. For the Z-boson analysis, two muon candidates with a transverse momentum of $p_T \gtrsim 0.5$ GeV/c are required, in coincidence with a MB event. The trigger selection on the muon p_T is not sharp and the threshold is defined as the value for which the trigger efficiency reaches a value of 50%. The integrated luminosities used in the analysis were computed by estimating the equivalent number of MB events corresponding to the muon-triggered data samples and then dividing by the MB cross sections. The latter were measured with Van der Meer scans and amount to 2.12 ± 0.07 b and 2.09 ± 0.07 b for the Pb-going and p-going samples, respectively [31]. The number of MB events corresponding to the

Centrality class	0–100%	2–20%	20–40%	40–60%	60–100%
$\langle N_{\text{coll}}^{\text{mult}} \rangle$	6.9 ± 0.6	11.3 ± 0.3	9.6 ± 0.2	7.1 ± 0.3	3.2 ± 0.1

Table 1: Average number of binary nucleon-nucleon collisions $\langle N_{\text{coll}}^{\text{mult}} \rangle$ estimated with the hybrid ZN method [28].

muon-triggered data sample is evaluated as $N_{\text{MB}} = F_{\mu\text{-trig}/\text{MB}} \cdot N_{\mu\text{-trig}}$ where $N_{\mu\text{-trig}}$ is the number of muon-triggered events and $F_{\mu\text{-trig}/\text{MB}}$ is the inverse probability of having a muon-triggered event in a MB event. The normalisation factor $F_{\mu\text{-trig}/\text{MB}}$ is estimated by using the information of the counters recording the total number of triggers, corrected for pile-up effects, which amount to 2%. The $F_{\mu\text{-trig}/\text{MB}}$ factor can also be obtained by applying the muon trigger condition in the analysis of MB events. The difference between the results obtained with the two methods, which amounts to about 1%, is taken as the systematic uncertainty. The integrated luminosity was also independently measured using the T0 detector: the results agree within better than 1% in both data samples. The difference was included in the systematic uncertainty of the MB cross section. The resulting luminosity is $5.81 \pm 0.20 \text{ nb}^{-1}$ and $5.03 \pm 0.18 \text{ nb}^{-1}$ for the Pb-going and p-going data samples, respectively.

The centrality of the collision is measured from the energy deposited in the ZN in the direction of the fragmenting lead ion. The average number of binary nucleon-nucleon collisions $\langle N_{\text{coll}} \rangle$ is obtained from the “hybrid method” described in [28], which relies on the assumption that the charged-particle multiplicity measured at mid-rapidity is proportional to the average number of nucleons participating in the interaction $\langle N_{\text{part}} \rangle$. The values of $\langle N_{\text{part}} \rangle$ for a given ZN-centrality class are calculated by scaling the average number of participants in MB collisions $\langle N_{\text{part}}^{\text{MB}} \rangle$, estimated with a Glauber Monte Carlo [32], by the ratio of the average charged-particle multiplicity measured at mid-rapidity for the ZN-centrality class and that of MB. These values are denoted as $\langle N_{\text{part}}^{\text{mult}} \rangle$ in the following to indicate the assumption used for the scaling. The corresponding number of binary collisions is then obtained as: $\langle N_{\text{coll}}^{\text{mult}} \rangle = \langle N_{\text{part}}^{\text{mult}} \rangle - 1$. The systematic uncertainties are estimated by using different ansätze, as described in [28]. The resulting values of $\langle N_{\text{coll}}^{\text{mult}} \rangle$ and their uncertainties are summarised in Table 1.

The muon trigger efficiency is found to be independent of centrality in p–Pb collisions. The normalisation factor of muon-triggered to MB events per centrality class can be obtained from the centrality integrated value $F_{\mu\text{-trig}/\text{MB}}$ scaled by the fraction of the MB events in the given centrality class. The 0–2% most central collisions are excluded in the centrality-dependent analysis, because of the large pile-up contamination in this event class (of the order of 20–30%). In pile-up events the ZN energies of two (or more) interactions sum up, thus biasing the centrality determination towards the most central classes. The contamination is reduced with decreasing centrality, and is about 3% in the 2–20% event classes in both the p-going and Pb-going data sample. These values are taken into account in the systematic uncertainties on the normalisation.

2.2 Muon selection and Monte Carlo simulations

Muon track candidates are reconstructed in the tracking system using the algorithm described in [33]. A fiducial cut on the pseudorapidity of the muon of $-4 < \eta < -2.5$ is applied in order to remove the particles at the edge of the spectrometer acceptance. An additional selection on the polar angle measured at the end of the front absorber of $170^\circ < \theta_{\text{abs}} < 178^\circ$ is required to reject muons crossing the high-density region of the front absorber that undergo significant scattering. Muon identification is carried out by matching the tracks reconstructed in the tracker and the trigger systems. The contamination from beam-induced background tracks, which do not point to the interaction vertex, can be efficiently removed by exploiting the correlation between the momentum (p) of the track and its Distance of Closest Approach (DCA) to the vertex. Due to the multiple scattering in the front absorber, the DCA distribution of particles produced in the collision can be described with a Gaussian function, whose width depends on the material crossed and is proportional to $1/p$. On the other hand, the background tracks have a DCA larger than about 40 cm, independent of p_{T} . They can therefore be rejected by selecting particles

with a p -DCA smaller than 6 times the width of the distribution, extracted from a Gaussian fit. The contamination depends on the beam configuration, being of the order of 7% in the p-going direction and up to 90% in the Pb-going direction for particles with $p_T > 10$ GeV/ c . However, in this region the signal and the background are completely separated and the selection can fully remove the background, with a signal rejection smaller than 0.3%.

The probability of a cosmic muon to be reconstructed in coincidence with a minimum bias trigger is very small, of the order of 10^{-10} . The selection on the p -DCA of the track further reduces the contamination to a negligible level.

The detector response for muons from W and Z boson decays was determined through Monte Carlo (MC) simulations. The W and Z bosons are produced using POWHEG [34], a NLO particle generator, paired with PYTHIA 6.425 [35] for parton shower. The calculations include the CT10 [36] PDF set and the EPS09NLO [25] parameterisation of the nuclear modification of the PDFs. The propagation of particles through the detector and the absorption materials uses the GEANT3 [37] transport code. The simulation of p–Pb collisions takes into account the isospin dependence (in terms of u- and d-type quark content) of the W and Z boson production, which is particularly important for W bosons [38]. To this aim proton–proton (pp) and proton–neutron (pn) collisions are simulated separately. The p–Pb collisions are obtained as the sum of the results, weighted by the average number of pp and pn interactions in a p–Pb collision.

The alignment of the tracking chambers is a crucial step in the analysis of muons at high transverse momentum. The absolute position of the chambers was measured before data taking with photogrammetry. Their relative position is estimated with a precision of about 100 μm , using a modified version of the MILLIPEDE [39] package, which combines data taken with and without the magnetic field. The residual misalignment of the tracking chambers is taken into account in the simulations to estimate the acceptance and efficiency ($A \times \varepsilon$) of the detector. While the method provides the most accurate estimation of the relative chamber position, it is not sensitive to a global misalignment of the entire spectrometer. A data-driven method was hence developed, in which the simulation of the tracker response is based on a parameterisation of the measured resolution of the clusters associated to a track. The distribution of the difference between the cluster and the reconstructed track positions on each chamber is parameterised with an extended Crystal-Ball function [40] and utilised to simulate the smearing of the track parameters. The effect of a global misalignment of the muon spectrometer is mimicked by shifting the distribution of the track deviation in the magnetic field in opposite directions for positive and negative tracks. This shift is tuned so as to reproduce the observed difference in the ratio of the p_T distributions of positive and negative tracks, corrected for acceptance and efficiency, in two periods of data taking differing only by the magnetic field polarity. The values of the $A \times \varepsilon$ corrections are obtained using either the standard simulations with the residual misalignment, or the data-driven simulations: the difference is about 1% (2%) in the p-going (Pb-going) data sample for Z bosons, and about 1% for W bosons. These values are taken as the systematic uncertainties. It is worth noting that the limited momentum resolution of the detector can also result in positive muons wrongly reconstructed as negative muons and viceversa. The resulting loss of efficiency is small (smaller than 1% for muons with $p_T > 10$ GeV/ c) and taken into account in the simulations.

The uncertainty on the muon tracking efficiency is estimated from the difference between the muon tracking efficiency in MC and that from a data-driven approach based on the redundancy of the tracking stations [41]. It amounts to 2% (3%) for the p-going (Pb-going) period. The uncertainty on trigger efficiency, which is mainly due to the systematic uncertainty in the determination of the efficiency of each trigger chamber from data, amounts to 1%. An additional systematic uncertainty of 0.5% results from the choice of the χ^2 cut in the matching of the tracks reconstructed in the tracker with those in the trigger. In the dimuon analysis, these systematic uncertainties apply to both muons of the pair, which are well separated in phase space and therefore cross different parts of the detector.

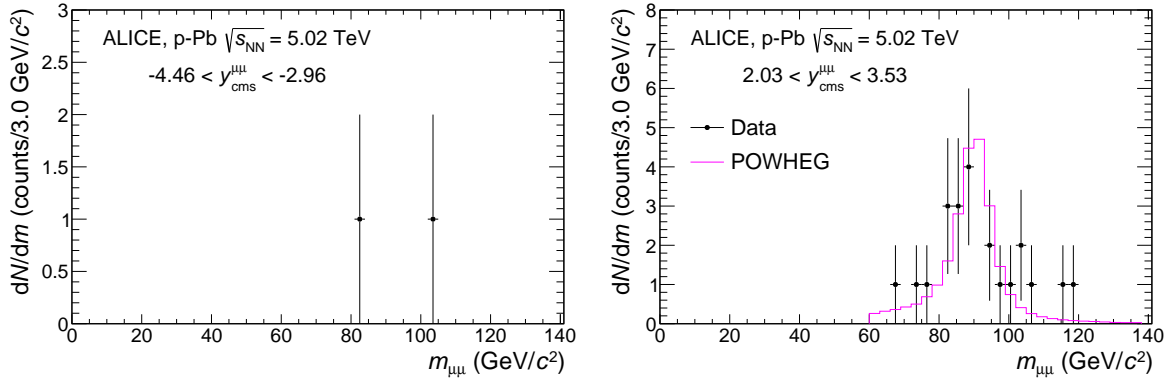


Fig. 1: Invariant-mass distribution of unlike-sign muon pairs with $p_T > 20$ GeV/ c in the Pb-going (left panel) and p-going (right panel) data samples. In the p-going one, the solid line represents the distribution obtained using POWHEG simulations and normalised to the number of Z candidates in the data.

2.3 Z-boson analysis

Z-boson candidates are obtained by combining opposite-charge pairs of muons, selected according to the criteria described in Section 2.2 and with a transverse momentum larger than 20 GeV/ c . This condition reduces the contribution of lower mass resonances and of the semi-leptonic decay of charm and beauty hadrons. It was verified that relaxing the requirement on the minimum p_T of the muon to 10 GeV/ c does not introduce any additional unlike-sign dimuon pair with $m_{\mu\mu} > 40$ GeV/ c^2 . The resulting invariant-mass distribution is shown in Fig. 1. There are 2 (22) candidates with $m_{\mu\mu} > 60$ GeV/ c^2 reconstructed in the Pb-going (p-going) period.

For the p-going data sample, where the number of dimuons is larger, the distribution is compared with expectations from the POWHEG MC simulations described in Section 2.2. The results are shown in the right panel of Fig. 1.

The contribution to the invariant-mass distribution from combinatorial background can be estimated using the like-sign dimuon distribution: no candidates were found in the region $60 < m_{\mu\mu} < 120$ GeV/ c^2 . A 0.1% upper limit for this contribution is obtained by extrapolating the like-sign dimuon distribution at low mass ($m_{\mu\mu} < 20$ GeV/ c^2) to the region of interest. Contributions from other physics processes, like the semileptonic decays of $c\bar{c}$, $b\bar{b}$ and $t\bar{t}$ pairs and the muonic decay of τ pairs is estimated to be less than 0.7% (0.4%) for the p-going (Pb-going) data taking period. Those estimations were done using MC simulations (PYTHIA 6.425 for the first process and POWHEG for the others). Since no background events are expected, the number of Z candidates is obtained by counting the entries in the invariant-mass distributions of opposite-charge muon pairs of Fig. 1.

The measured number of candidates is corrected by the $A \times \varepsilon$ evaluated with simulations. The $A \times \varepsilon$ is estimated as the ratio of the number of reconstructed Z bosons with the same analysis cuts used in data to the number of generated ones with $-4 < \eta < -2.5$ and $p_T^\mu > 20$ GeV/ c . An invariant mass cut of $60 < m_{\mu\mu} < 120$ GeV/ c^2 is applied to both reconstructed and generated Z bosons. The resulting $A \times \varepsilon$ is 78% (61%) for the p-going (Pb-going) data taking period, with a relative systematic uncertainty of 1% (2%). The lower $A \times \varepsilon$ value in the Pb-going configuration is due to a smaller detector efficiency in the corresponding data-taking period. The uncertainty accounts for the difference from the values obtained with a simulation based on the residual misalignment and that based on the data-driven alignment. The systematic uncertainties are summarised in Table 2.

2.4 W-boson analysis

At transverse momenta higher than 10 GeV/ c , the main contributions to the inclusive p_T distribution of muons are the decays of W bosons, the dimuon decays of Z bosons and the muon decays of heavy-

Background contamination	< 1%
Tracking efficiency	4% (p-going) 6% (Pb-going)
Trigger efficiency	2%
Tracker/trigger matching	1%
Alignment	1% (p-going) 2% (Pb-going)
$F_{\mu\text{-trig/MB}}$	1%
MB cross section	3.3%

Table 2: Summary of systematic uncertainties for Z-boson analysis.

flavoured hadrons. The number of muons from W decays can be extracted from the inclusive p_T spectrum before $A \times \varepsilon$ corrections through a fit procedure based on MC template descriptions of these three main components:

$$f(p_T) = N_{\text{bkg}}^{\text{raw}} f_{\text{bkg}}(p_T) + N_{\mu \leftarrow W}^{\text{raw}} (f_{\mu \leftarrow W}(p_T) + R f_{\mu \leftarrow Z}(p_T)) \quad (1)$$

where f_{bkg} , $f_{\mu \leftarrow W}$ and $f_{\mu \leftarrow Z}$ are the MC templates for muons from heavy-flavoured hadrons, W-boson and Z-boson decays, respectively. The number of muons from heavy-flavour decays ($N_{\text{bkg}}^{\text{raw}}$) and the number of muons from W decays ($N_{\mu \leftarrow W}^{\text{raw}}$) are free parameters, while the ratio (R) of the number of muons from Z decays and that from W decays is fixed from MC simulations using POWHEG. It was verified that these calculations well describe the measured Z boson production in the dimuonic decay channel, described in the previous section. The contribution of muons from heavy-flavour decays was simulated using as input the QCD calculations in the Fixed-Order Next-to-Leading-Log (FONLL) approach [42], which are found to provide a good description of data in pp collisions. The calculations were obtained using the CTEQ6.6 parton distribution functions [43], without accounting for any nuclear modification. Such modifications, however, mainly affect the production at low transverse momenta, with a negligible effect in the shape of the p_T distribution in the region of interest for this study [44]. The templates for muons from the decay of W and Z bosons were obtained with MC simulations based on POWHEG. The detector response is included in all simulations.

The inclusive transverse momentum distributions of positive and negative muon candidates passing the selections described in Section 2.2 are fitted according to Eq. 1, and the parameter $N_{\mu \leftarrow W}^{\text{raw}}$ is extracted from the fit. The MC templates are then modified as explained later on to account for the uncertainties affecting their shape and the fit is performed again, thus yielding different values of $N_{\mu \leftarrow W}^{\text{raw}}$. The procedure is reiterated for each set of MC templates considered. The number of muons from W decays is finally estimated as the arithmetic average of the $N_{\mu \leftarrow W}^{\text{raw}}$ extracted in each fit, while their dispersion, estimated as the Root Mean Square (RMS) of the $N_{\mu \leftarrow W}^{\text{raw}}$ distribution, is used as systematic uncertainty. An example of signal extraction for a specific set of MC templates is shown in Fig. 2.

Several sources of uncertainty affecting the shape of the MC templates were taken into account. For the background, different MC templates were obtained by varying the FONLL calculations within uncertainties. In particular, six additional templates were produced, corresponding to the upper and lower limits of the calculations obtained by i) varying the factorisation and renormalisation scales, and considering the uncertainties on ii) the quark masses and iii) the PDFs. For the W and Z boson production, different PDF sets were used, both at LO and NLO, in particular the CT10 [36] and CTEQ6 [45] paired with EPS09. The use of different sets affects both the shapes of the templates and the cross-sections, thus resulting in a variation of the parameter R in Eq. 1. The stability of the fit was tested by varying the lower limit of the transverse momentum range (the upper one being mainly limited by statistics) from 15 to 17 GeV/ c . Finally, the effect of the momentum resolution was accounted for by using two different sets of templates for each MC input, obtained by including in the simulations either the tracking chamber residual misalignment or the data-driven method discussed in Section 2.2. The contamination to the positive muon spectrum of negative muons with mis-identified charge sign (and viceversa) is estimated to be smaller than 1% for $p_T > 10$ GeV/ c . The contamination depends on the p_T , but the resulting variation of the

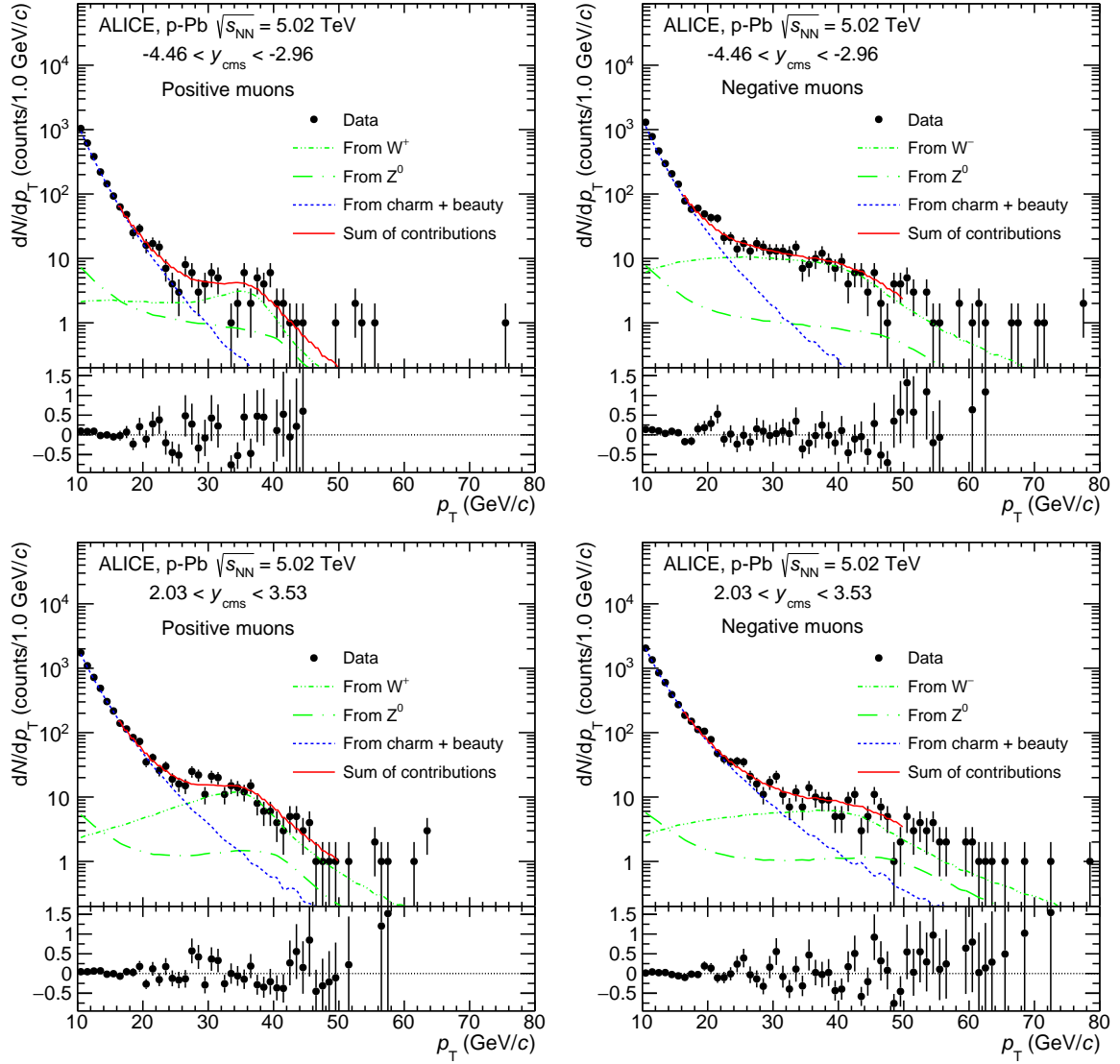


Fig. 2: Top panels: inclusive distribution of positive (left) and negative (right) charge muon candidates measured in the Pb-going (top) and p-going (bottom) data taking periods. The results of the MC template fit for the extraction of the $\mu^+ \leftarrow W^+$ and $\mu^- \leftarrow W^-$ signal is shown. In this case, the central value of the FONLL calculations is used for the background description while POWHEG with the CT10 PDF set paired with EPS09NLO is used for W and Z boson production. Bottom panels: relative difference of data and the extrapolated fit results in the range $10 < p_T < 80$ GeV/c.

yields in the p_T range of the fit is found to be smaller than the variation of the shape of the templates obtained with different descriptions of the alignment.

The number of muons from W-boson decays is then corrected for the detector acceptance and efficiency. The values of $A \times \varepsilon$ integrated over $p_T^\mu > 10$ GeV/c are 89% for μ^+ and 88% for μ^- in the p-going period and of 77% for μ^+ and 75% for μ^- in the Pb-going period. The lower $A \times \varepsilon$ value in the Pb-going configuration is due to a smaller detector efficiency in the corresponding data-taking period. A difference of 1% in the values is observed when using the data-driven method for the description of the alignment in the simulations instead of the residual misalignment. This value is taken as the systematic uncertainty.

All systematic uncertainties are summarised in Table 3.

Signal extraction	2 – 6%
- vs centrality	5 – 15%
Tracking efficiency (c)	2% (p-going) 3% (Pb-going)
Trigger efficiency (c)	1%
Tracker/trigger matching (c)	0.5%
Alignment (c)	1%
$F_{\mu\text{-trig}/\text{MB}}$ (c)	1%
MB cross section (c)	3.3%
Pile-up	1 - 3 %
$\langle N_{\text{coll}}^{\text{mult}} \rangle$	2 – 8%

Table 3: Summary of systematic uncertainties for W-boson analysis. The uncertainties that are correlated between measurements in different centrality bins are indicated with (c).

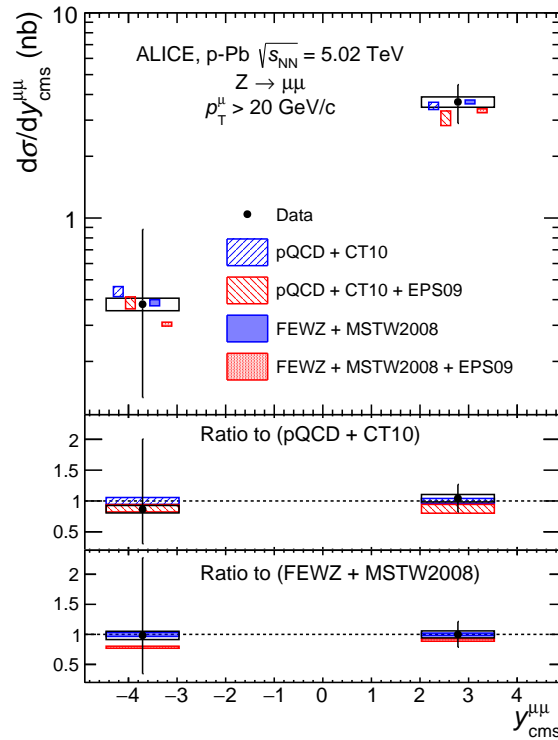


Fig. 3: Z-boson production cross section in the dimuon decay channel at backward and forward rapidities measured in p–Pb collisions at $\sqrt{s_{NN}} = 5.02$ TeV. The vertical error bars (open boxes) represent the statistical (systematic) uncertainties. The horizontal width of the boxes corresponds to the measured rapidity range. The results are compared with theoretical calculations [26, 46] performed both with and without including the nuclear modification of the parton distribution functions. In the top panel, the calculations are shifted along the rapidity axis to improve the visibility. The middle (bottom) panel shows the data and pQCD (FEWZ) calculations divided by the pQCD (FEWZ) calculations without nuclear modification of the PDFs.

3 Results

The Z-boson production cross section in the dimuon decay channel with $p_T^\mu > 20$ GeV/c and $60 < m_{\mu\mu} < 120$ GeV/c² is shown in Fig. 3. The vertical bars represent the statistical uncertainties while the open boxes are the systematic ones. The cross section at backward rapidity is estimated from two reconstructed Z boson candidates (see left panel of Fig. 1). In this case, the statistical uncertainty is defined as the 68% confidence interval assuming a Poisson distribution for the number of Z bosons. Moreover, an upper limit was also calculated, whose value is of 1.75 nb at a 95% confidence level. The

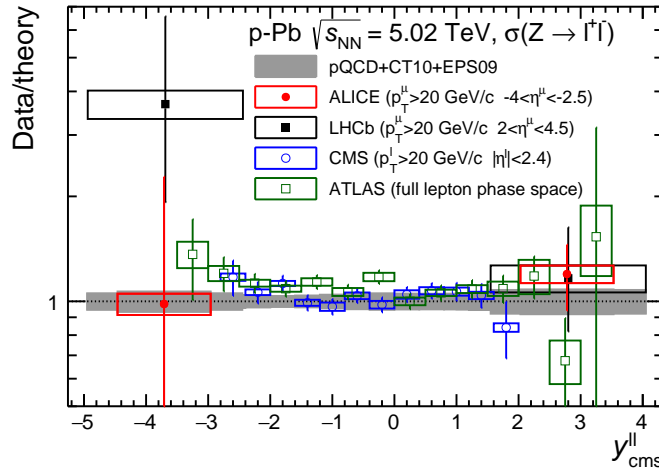


Fig. 4: Ratio of data over theoretical calculations for the Z-boson production cross section measured by the ALICE, LHCb [18], ATLAS [16] and CMS [17] experiments. The LHCb points have been shifted by +0.02 units of rapidity for better visibility. The ATLAS cross sections are measured in a slightly smaller invariant mass range ($66 < m_{ll} < 116$ GeV/c²) compared to the other experiments ($60 < m_{ll} < 120$ GeV/c²). The luminosity uncertainties of 2.7% for ATLAS and 3.5% for CMS are not shown. The pQCD calculations are obtained with the CT10 PDF set and with the EPS09NLO parameterisation of the nuclear modifications.

results are compared with NLO and NNLO theoretical calculations both with and without including the nuclear modification of the parton distribution functions. The NLO pQCD calculations [26] (blue hatched boxes) are obtained using the CT10 [36] PDF, while the NNLO calculations with FEWZ [46] (blue filled boxes) use the MSTW2008 NNLO [47] PDF set. Both calculations describe the data within uncertainties. The corresponding calculations with the EPS09NLO parameterisation of the nuclear modification of the parton distribution functions are shown as hatched and filled red boxes, respectively. The nuclear effect results in a small reduction of the cross section, in particular at forward rapidities where lower Bjorken- x values of the Pb nucleons are probed. The effect, however, is small and the measurement is compatible with both calculations within uncertainties.

The Z-boson production cross section was measured in p–Pb collisions at $\sqrt{s_{NN}} = 5.02$ TeV by the ATLAS and CMS experiments at mid-rapidity [16, 17] and by the LHCb experiment at forward and backward rapidities [18]. The LHCb measurement is performed in a wider pseudorapidity interval ($2 < \eta < 4.5$) compared to ALICE, but on a data sample with a smaller integrated luminosity. Figure 4 shows the cross section measurements of the four LHC experiments, each divided by the corresponding NLO pQCD expectation including the nuclear modification of the PDFs [26]: the calculations are found to describe all data. It is worth noting, however, that none of the experiments can exclude the calculations without nPDFs.

The cross sections of muons from W^+ and W^- boson decays with $p_T^\mu > 10$ GeV/c measured at forward and backward rapidities in p–Pb collisions at $\sqrt{s_{NN}} = 5.02$ TeV are shown in the left and right panels of Fig. 5, respectively. The vertical bars represent the statistical uncertainties while the open boxes are the systematic ones. The smaller cross-section of positive W bosons at backward rapidity is the combined effect of the parity violation of the weak interaction, which only couples left-handed fermions with right-handed anti-fermions, and of the helicity conservation in the leptonic decay. This results in an anisotropic emission of the muons. In particular, the μ^- is preferably emitted in the same direction of the W^- , while the μ^+ is emitted in the opposite direction with respect to the W^+ [38]. This implies that the μ^+ measured in $-4.46 < y_{cms} < -2.96$ mainly comes from the decay of W^+ at even more backward rapidities, where the production cross-section rapidly decreases.

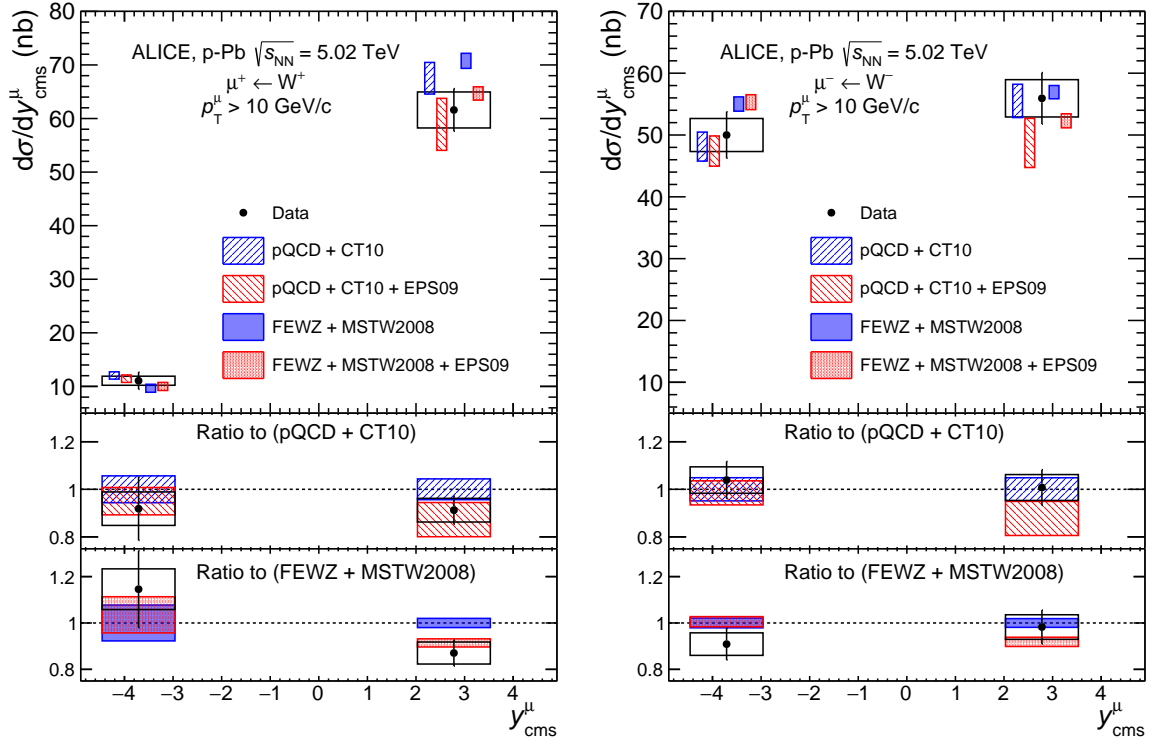


Fig. 5: Left (right) panel: cross section of μ^+ (μ^-) from W^+ (W^-) boson decays at backward and forward rapidities measured in p–Pb collisions at $\sqrt{s_{\text{NN}}} = 5.02$ TeV. The vertical error bars (open boxes) represent the statistical (systematic) uncertainties. The horizontal width of the boxes corresponds to the measured rapidity range. The results are compared with theoretical calculations [26, 46] performed both with and without including the nuclear modification of the parton distribution functions. In the top panels, the calculations are shifted along the rapidity axis to improve the visibility. The middle (bottom) panel shows the data and pQCD (FEWZ) calculations divided by the pQCD (FEWZ) calculations without nuclear modification of the PDFs.

The results are compared with the analogous model calculations used to describe the Z-boson production. The NLO pQCD calculations with CT10 parton distribution functions (blue hatched boxes) and the NNLO calculations with FEWZ with the MSTW2008 PDF set (blue filled boxes) both describe the data within uncertainties. The inclusion of a parameterisation of the nuclear modification of the parton distribution function in the calculations (red hatched boxes for pQCD and red filled boxes for FEWZ) results in a slightly lower value of the cross section, especially at forward rapidity. This variation, however, is of the same order as the uncertainties in the theoretical calculations, thus limiting the discriminating power of the cross section alone.

The asymmetry in the production of the W^+ and W^- bosons can be used to gain sensitivity in the study of the nuclear modification of the PDFs [19]. Part of the theoretical uncertainties, such as those on the factorization and renormalization scale that are of the order of 5%, and the experimental uncertainties on the tracking and trigger efficiency, normalisation factors and MB cross section, whose quadratic sum amounts to 4.3% (4.8%) in the p-going (Pb-going) period, cancel when measuring the relative yield of muons from W^+ and W^- decays. Figure 6 shows the lepton charge asymmetry, which is defined as:

$$\frac{N_{\mu^+\leftarrow W^+} - N_{\mu^-\leftarrow W^-}}{N_{\mu^+\leftarrow W^+} + N_{\mu^-\leftarrow W^-}} \quad (2)$$

where $N_{\mu^+\leftarrow W^+}$ and $N_{\mu^-\leftarrow W^-}$ are the yields of muons from, respectively, the W^+ and W^- decays, corrected by the detector acceptance and efficiency. The relative systematic uncertainties in the pQCD and FEWZ calculations are strongly reduced in the ratio. However, the model results with and without nu-

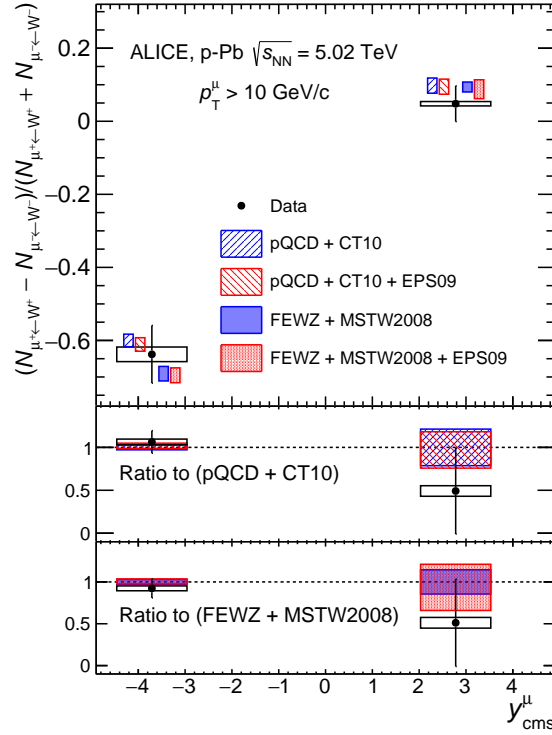


Fig. 6: Lepton charge asymmetry of muons from W-boson decays at backward and forward rapidities measured in p–Pb collisions at $\sqrt{s_{NN}} = 5.02$ TeV. The vertical error bars (open boxes) represent the statistical (systematic) uncertainties. The horizontal width of the boxes corresponds to the measured rapidity range. The results are compared with theoretical calculations [26, 46] performed both with and without including the nuclear modification of the parton distribution functions. In the top panel, the calculations are shifted along the rapidity axis to improve the visibility. The middle (bottom) panel shows the data and pQCD (FEWZ) calculations divided by the pQCD (FEWZ) calculations without nuclear modification of the PDFs.

clear modification are very similar in this kinematic range, and the measurement cannot discriminate between them.

The production of electrons and muons from W-boson decays was measured at mid-rapidity in p–Pb collisions at $\sqrt{s_{NN}} = 5.02$ TeV by the CMS experiment [19]. The cross section results, each divided by the corresponding NLO pQCD expectation including nuclear modification of the PDFs, are shown together with the analogous ALICE results in Fig. 7: the calculations are found to describe data over the full explored rapidity interval.

The production of muons from W-boson decays with $p_T^\mu > 10$ GeV/c is studied as a function of the collision centrality. Due to the limited statistics, the μ^+ and μ^- results are summed together. The resulting cross sections at backward and forward rapidities normalised by the average number of binary collisions [28] are shown in the left and right panels of Fig. 8, respectively. The vertical bars represent the statistical uncertainties while the open boxes are the uncorrelated systematic ones. The quadratic sum of the correlated systematic uncertainties on the MB cross section, normalisation, $A \times \epsilon$ correction and tracking and trigger efficiency, which amounts to 4.8% (4.3%) in the Pb-going (p-going) sample, are quoted in the figure.

As discussed in the introduction, if the W boson production rate is consistent with geometric expectation, the production cross-section is expected to scale with the number of binary collisions for all centrality classes, provided that the centrality determination is not biased. The measured centrality dependence is found to be compatible with a constant within uncertainties.

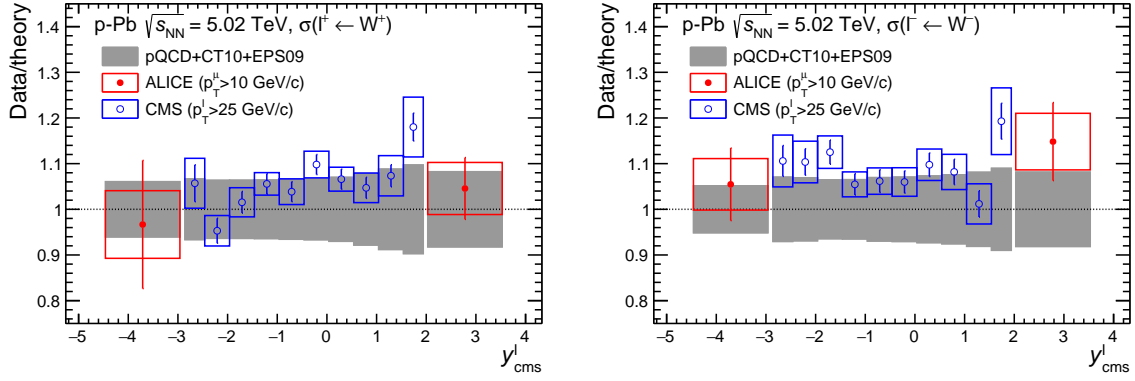


Fig. 7: Ratio of data over theoretical calculations for the production cross section of positive (left panel) and negative (right panel) muons and leptons from W-boson production measured by the ALICE and CMS experiments [19], respectively. The luminosity uncertainty of 3.5% for CMS is not shown. The pQCD calculations are obtained with CT10 NLO PDF set and with the EPS09NLO parameterisation of the nuclear modifications.

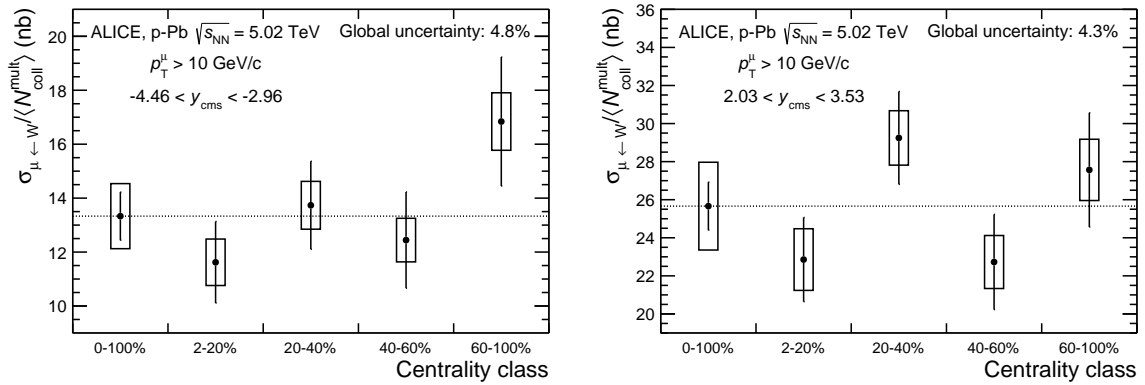


Fig. 8: Sum of the cross sections of positive and negative charge muons from W boson decays measured in p–Pb collisions at $\sqrt{s_{NN}} = 5.02$ TeV in the rapidity region $-4.46 < y_{\text{cms}} < -2.96$ (left panel) and $2.03 < y_{\text{cms}} < 3.53$ (right panel) as a function of centrality. The cross sections are normalised by the number of binary collisions $\langle N_{\text{coll}}^{\text{mult}} \rangle$. The vertical bars (open boxes) represent the statistical (systematic) uncertainties. The correlated global uncertainties include the MB cross section, normalisation, $A \times \epsilon$ corrections and tracking and trigger systematics. A dotted line is drawn at the value of the centrality-integrated cross section to guide the eye.

4 Summary

The ALICE experiment has studied the W and Z-boson production at forward and backward rapidities in p–Pb collisions at $\sqrt{s_{NN}} = 5.02$ TeV at the LHC. The Z-boson cross section was measured in the dimuon decay channel with $p_T^\mu > 20$ GeV/c and $60 < m_{\mu\mu} < 120$ GeV/c². The W-boson cross section and decay lepton charge asymmetry were measured in the muonic decay channel with $p_T^\mu > 10$ GeV/c. The results are described by NLO pQCD calculations [26] as well as NNLO calculations using FEWZ [46], but the uncertainties on the measurement cannot constrain the nuclear modification of the PDFs. W-boson production was also measured as a function of the event centrality, estimated from the energy deposited in the neutron zero degree calorimeters. The cross section of muons from W-boson decays normalised by the number of binary nucleon-nucleon collisions is compatible with a constant within uncertainties. Further measurements with better precision are needed to provide more stringent constraints on the nPDFs and on the binary scaling.

Acknowledgements

The ALICE collaboration would like to thank Hannu Paukkunen for providing the pQCD calculations. The ALICE Collaboration would like to thank all its engineers and technicians for their invaluable contributions to the construction of the experiment and the CERN accelerator teams for the outstanding performance of the LHC complex. The ALICE Collaboration gratefully acknowledges the resources and support provided by all Grid centres and the Worldwide LHC Computing Grid (WLCG) collaboration. The ALICE Collaboration acknowledges the following funding agencies for their support in building and running the ALICE detector: A. I. Alikhanyan National Science Laboratory (Yerevan Physics Institute) Foundation (ANSL), State Committee of Science and World Federation of Scientists (WFS), Armenia; Austrian Academy of Sciences and Nationalstiftung für Forschung, Technologie und Entwicklung, Austria; Conselho Nacional de Desenvolvimento Científico e Tecnológico (CNPq), Universidade Federal do Rio Grande do Sul (UFRGS), Financiadora de Estudos e Projetos (Finep) and Fundação de Amparo à Pesquisa do Estado de São Paulo (FAPESP), Brazil; Ministry of Science & Technology of China (MSTC), National Natural Science Foundation of China (NSFC) and Ministry of Education of China (MOEC), China; Ministry of Science, Education and Sport and Croatian Science Foundation, Croatia; Ministry of Education, Youth and Sports of the Czech Republic, Czech Republic; The Danish Council for Independent Research — Natural Sciences, the Carlsberg Foundation and Danish National Research Foundation (DNRF), Denmark; Helsinki Institute of Physics (HIP), Finland; Commissariat à l’Energie Atomique (CEA) and Institut National de Physique Nucléaire et de Physique des Particules (IN2P3) and Centre National de la Recherche Scientifique (CNRS), France; Bundesministerium für Bildung, Wissenschaft, Forschung und Technologie (BMBF) and GSI Helmholtzzentrum für Schwerionenforschung GmbH, Germany; Ministry of Education, Research and Religious Affairs, Greece; National Research, Development and Innovation Office, Hungary; Department of Atomic Energy Government of India (DAE), India; Indonesian Institute of Science, Indonesia; Centro Fermi - Museo Storico della Fisica e Centro Studi e Ricerche Enrico Fermi and Istituto Nazionale di Fisica Nucleare (INFN), Italy; Institute for Innovative Science and Technology, Nagasaki Institute of Applied Science (IIST), Japan Society for the Promotion of Science (JSPS) KAKENHI and Japanese Ministry of Education, Culture, Sports, Science and Technology (MEXT), Japan; Consejo Nacional de Ciencia (CONACYT) y Tecnología, through Fondo de Cooperación Internacional en Ciencia y Tecnología (FONCICYT) and Dirección General de Asuntos del Personal Académico (DGAPA), Mexico; Nationaal instituut voor subatomaire fysica (Nikhef), Netherlands; The Research Council of Norway, Norway; Commission on Science and Technology for Sustainable Development in the South (COMSATS), Pakistan; Pontificia Universidad Católica del Perú, Peru; Ministry of Science and Higher Education and National Science Centre, Poland; Korea Institute of Science and Technology Information and National Research Foundation of Korea (NRF), Republic of Korea; Ministry of Education and Scientific Research, Institute of Atomic Physics and Romanian National Agency for Science, Technology and Innovation, Romania; Joint Institute for Nuclear Research (JINR), Ministry of Education and Science of the Russian Federation and National Research Centre Kurchatov Institute, Russia; Ministry of Education, Science, Research and Sport of the Slovak Republic, Slovakia; National Research Foundation of South Africa, South Africa; Centro de Aplicaciones Tecnológicas y Desarrollo Nuclear (CEADEN), Cubaenergía, Cuba, Ministerio de Ciencia e Innovación and Centro de Investigaciones Energéticas, Medioambientales y Tecnológicas (CIEMAT), Spain; Swedish Research Council (VR) and Knut & Alice Wallenberg Foundation (KAW), Sweden; European Organization for Nuclear Research, Switzerland; National Science and Technology Development Agency (NSDTA), Suranaree University of Technology (SUT) and Office of the Higher Education Commission under NRU project of Thailand, Thailand; Turkish Atomic Energy Agency (TAEK), Turkey; National Academy of Sciences of Ukraine, Ukraine; Science and Technology Facilities Council (STFC), United Kingdom; National Science Foundation of the United States of America (NSF) and United States Department of Energy, Office of Nuclear Physics (DOE NP), United States of America.

References

- [1] **UA1** Collaboration, C. Albajar *et al.*, “Intermediate Vector Boson Cross-Sections at the CERN Super Proton Synchrotron Collider and the Number of Neutrino Types,” *Phys. Lett.* **B198** (1987) 271.
- [2] **UA2** Collaboration, J. Alitti *et al.*, “A Measurement of the W and Z production cross-sections and a determination of $\Gamma(W)$ at the CERN $\bar{p}p$ collider,” *Phys. Lett.* **B276** (1992) 365–374.
- [3] **CDF** Collaboration, F. Abe *et al.*, “Measurement of $\sigma \cdot B(W \rightarrow e\nu)$ and $\sigma \cdot B(Z^0 \rightarrow e^+e^-)$ in $p\bar{p}$ collisions at $\sqrt{s} = 1.8$ TeV,” *Phys. Rev. Lett.* **76** (1996) 3070–3075, arXiv:hep-ex/9509010 [hep-ex].
- [4] **CDF** Collaboration, A. Abulencia *et al.*, “Measurements of inclusive W and Z cross sections in p anti- p collisions at $\sqrt{s} = 1.96$ TeV,” *J. Phys.* **G34** (2007) 2457–2544, arXiv:hep-ex/0508029 [hep-ex].
- [5] **D0** Collaboration, B. Abbott *et al.*, “Extraction of the width of the W boson from measurements of $\sigma(p\bar{p} \rightarrow W + X) \times B(W \rightarrow e\nu)$ and $\sigma(p\bar{p} \rightarrow Z + X) \times B(Z \rightarrow ee)$ and their ratio,” *Phys. Rev.* **D61** (2000) 072001, arXiv:hep-ex/9906025 [hep-ex].
- [6] **PHENIX** Collaboration, A. Adare *et al.*, “Cross Section and Parity Violating Spin Asymmetries of W^\pm Boson Production in Polarized $p + p$ Collisions at $\sqrt{s} = 500$ GeV,” *Phys. Rev. Lett.* **106** (2011) 062001, arXiv:1009.0505 [hep-ex].
- [7] **STAR** Collaboration, M. M. Aggarwal *et al.*, “Measurement of the parity-violating longitudinal single-spin asymmetry for W^\pm boson production in polarized proton-proton collisions at $\sqrt{s} = 500$ GeV,” *Phys. Rev. Lett.* **106** (2011) 062002, arXiv:1009.0326 [hep-ex].
- [8] **ATLAS** Collaboration, G. Aad *et al.*, “Measurement of the inclusive W^\pm and Z/γ cross sections in the electron and muon decay channels in pp collisions at $\sqrt{s} = 7$ TeV with the ATLAS detector,” *Phys. Rev.* **D85** (2012) 072004, arXiv:1109.5141 [hep-ex].
- [9] **ATLAS** Collaboration, G. Aad *et al.*, “Measurement of W^\pm and Z -boson production cross sections in pp collisions at $\sqrt{s} = 13$ TeV with the ATLAS detector,” *Phys. Lett.* **B759** (2016) 601–621, arXiv:1603.09222 [hep-ex].
- [10] **CMS** Collaboration, S. Chatrchyan *et al.*, “Measurement of the Inclusive W and Z Production Cross Sections in pp Collisions at $\sqrt{s} = 7$ TeV,” *JHEP* **10** (2011) 132, arXiv:1107.4789 [hep-ex].
- [11] **CMS** Collaboration, S. Chatrchyan *et al.*, “Measurement of inclusive W and Z boson production cross sections in pp collisions at $\sqrt{s} = 8$ TeV,” *Phys. Rev. Lett.* **112** (2014) 191802, arXiv:1402.0923 [hep-ex].
- [12] **LHCb** Collaboration, R. Aaij *et al.*, “Measurement of the forward Z boson production cross-section in pp collisions at $\sqrt{s} = 7$ TeV,” *JHEP* **08** (2015) 039, arXiv:1505.07024 [hep-ex].
- [13] **LHCb** Collaboration, R. Aaij *et al.*, “Measurement of forward W and Z boson production in pp collisions at $\sqrt{s} = 8$ TeV,” *JHEP* **01** (2016) 155, arXiv:1511.08039 [hep-ex].
- [14] U. Baur, S. Keller, and D. Wackerath, “Electroweak radiative corrections to W boson production in hadronic collisions,” *Phys. Rev.* **D59** (1999) 013002, arXiv:hep-ph/9807417 [hep-ph].

- [15] A. D. Martin, R. G. Roberts, W. J. Stirling, and R. S. Thorne, “Parton distributions and the LHC: W and Z production,” *Eur. Phys. J.* **C14** (2000) 133–145, arXiv:hep-ph/9907231 [hep-ph].
- [16] ATLAS Collaboration, G. Aad *et al.*, “Z boson production in p+Pb collisions at $\sqrt{s_{NN}} = 5.02$ TeV measured with the ATLAS detector,” *Phys. Rev.* **C92** no. 4, (2015) 044915, arXiv:1507.06232 [hep-ex].
- [17] CMS Collaboration, V. Khachatryan *et al.*, “Study of Z boson production in pPb collisions at $\sqrt{s_{NN}} = 5.02$ TeV,” *Phys. Lett.* **B759** (2016) 36–57, arXiv:1512.06461 [hep-ex].
- [18] LHCb Collaboration, R. Aaij *et al.*, “Observation of Z production in proton-lead collisions at LHCb,” *JHEP* **1409** (2014) 030, arXiv:1406.2885 [hep-ex].
- [19] CMS Collaboration, V. Khachatryan *et al.*, “Study of W boson production in pPb collisions at $\sqrt{s_{NN}} = 5.02$ TeV,” *Phys. Lett.* **B750** (2015) 565–586, arXiv:1503.05825 [nucl-ex].
- [20] ATLAS Collaboration, G. Aad *et al.*, “Measurement of the production and lepton charge asymmetry of W bosons in Pb+Pb collisions at $\sqrt{s_{NN}} = 2.76$ TeV with the ATLAS detector,” *Eur.Phys.J.* **C75** no. 1, (2015) 23, arXiv:1408.4674 [hep-ex].
- [21] ATLAS Collaboration, G. Aad *et al.*, “Measurement of Z boson Production in Pb+Pb Collisions at $\sqrt{s_{NN}} = 2.76$ TeV with the ATLAS Detector,” *Phys.Rev.Lett.* **110** no. 2, (2013) 022301, arXiv:1210.6486 [hep-ex].
- [22] CMS Collaboration, S. Chatrchyan *et al.*, “Study of W boson production in PbPb and pp collisions at $\sqrt{s_{NN}} = 2.76$ TeV,” *Phys.Lett.* **B715** (2012) 66–87, arXiv:1205.6334 [nucl-ex].
- [23] CMS Collaboration, S. Chatrchyan *et al.*, “Study of Z production in PbPb and pp collisions at $\sqrt{s_{NN}} = 2.76$ TeV in the dimuon and dielectron decay channels,” *JHEP* **1503** (2015) 022, arXiv:1410.4825 [nucl-ex].
- [24] D. de Florian, R. Sassot, P. Zurita, and M. Stratmann, “Global Analysis of Nuclear Parton Distributions,” *Phys. Rev.* **D85** (2012) 074028, arXiv:1112.6324 [hep-ph].
- [25] K. J. Eskola, H. Paukkunen, and C. A. Salgado, “EPS09: A New Generation of NLO and LO Nuclear Parton Distribution Functions,” *JHEP* **04** (2009) 065, arXiv:0902.4154 [hep-ph].
- [26] H. Paukkunen and C. A. Salgado, “Constraints for the nuclear parton distributions from Z and W production at the LHC,” *JHEP* **1103** (2011) 071, arXiv:1010.5392 [hep-ph].
- [27] I. Helenius, K. J. Eskola, H. Honkanen, and C. A. Salgado, “Impact-Parameter Dependent Nuclear Parton Distribution Functions: EPS09s and EKS98s and Their Applications in Nuclear Hard Processes,” *JHEP* **07** (2012) 073, arXiv:1205.5359 [hep-ph].
- [28] ALICE Collaboration, J. Adam *et al.*, “Centrality dependence of particle production in p-Pb collisions at $\sqrt{s_{NN}} = 5.02$ TeV,” *Phys.Rev.* **C91** no. 6, (2015) 064905, arXiv:1412.6828 [nucl-ex].
- [29] ALICE Collaboration, K. Aamodt *et al.*, “The ALICE experiment at the CERN LHC,” *JINST* **3** (2008) S08002.
- [30] ALICE Collaboration, E. Abbas *et al.*, “Performance of the ALICE VZERO system,” *JINST* **8** (2013) P10016, arXiv:1306.3130 [nucl-ex].
- [31] ALICE Collaboration, B. B. Abelev *et al.*, “Measurement of visible cross sections in proton-lead collisions at $\sqrt{s_{NN}} = 5.02$ TeV in van der Meer scans with the ALICE detector,” *JINST* **9** no. 11, (2014) P11003, arXiv:1405.1849 [nucl-ex].

- [32] M. L. Miller, K. Reygers, S. J. Sanders, and P. Steinberg, “Glauber modeling in high energy nuclear collisions,” *Ann. Rev. Nucl. Part. Sci.* **57** (2007) 205–243, arXiv:nucl-ex/0701025 [nucl-ex].
- [33] ALICE Collaboration, K. Aamodt *et al.*, “Rapidity and transverse momentum dependence of inclusive J/ψ production in pp collisions at $\sqrt{s} = 7$ TeV,” *Phys. Lett.* **B704** (2011) 442–455, arXiv:1105.0380 [hep-ex]. [Erratum: *Phys. Lett.* B718,692(2012)].
- [34] S. Alioli, P. Nason, C. Oleari, and E. Re, “NLO vector-boson production matched with shower in POWHEG,” *JHEP* **07** (2008) 060, arXiv:0805.4802 [hep-ph].
- [35] T. Sjostrand, S. Mrenna, and P. Z. Skands, “PYTHIA 6.4 Physics and Manual,” *JHEP* **05** (2006) 026, arXiv:hep-ph/0603175 [hep-ph].
- [36] H.-L. Lai, M. Guzzi, J. Huston, Z. Li, P. M. Nadolsky, J. Pumplin, and C. P. Yuan, “New parton distributions for collider physics,” *Phys. Rev.* **D82** (2010) 074024, arXiv:1007.2241 [hep-ph].
- [37] R. Brun, F. Carminati, and S. Giani, “GEANT Detector Description and Simulation Tool,” *CERN-W-5013* (1994).
- [38] Z. Conesa Del Valle, *Performance of the ALICE muon spectrometer. Weak boson production and measurement in heavy-ion collisions at LHC*. PhD thesis, SUBATECH, Nantes, 2007. <http://inspirehep.net/record/886889/files/CERN-THESIS-2007-102.pdf>.
- [39] V. Blobel and C. Kleinwort, “A New method for the high precision alignment of track detectors,” in *Advanced statistical techniques in particle physics. Proceedings, Conference, Durham, UK, March 18-22, 2002*, pp. URL–STR(9). 2002. arXiv:hep-ex/0208021 [hep-ex]. <http://www.ipp.dur.ac.uk/Workshops/02/statistics/proceedings//blobel1.pdf>.
- [40] J. Gaiser, *Charmonium Spectroscopy From Radiative Decays of the J/ψ and ψ'* . PhD thesis, SLAC, 1982. <http://slac.stanford.edu/pubs/slacreports/reports02/slac-r-255.pdf>.
- [41] ALICE Collaboration, B. B. Abelev *et al.*, “Performance of the ALICE Experiment at the CERN LHC,” *Int. J. Mod. Phys.* **A29** (2014) 1430044, arXiv:1402.4476 [nucl-ex].
- [42] M. Cacciari, S. Frixione, N. Houdeau, M. L. Mangano, P. Nason, and G. Ridolfi, “Theoretical predictions for charm and bottom production at the LHC,” *JHEP* **10** (2012) 137, arXiv:1205.6344 [hep-ph].
- [43] P. M. Nadolsky, H.-L. Lai, Q.-H. Cao, J. Huston, J. Pumplin, D. Stump, W.-K. Tung, and C. P. Yuan, “Implications of CTEQ global analysis for collider observables,” *Phys. Rev.* **D78** (2008) 013004, arXiv:0802.0007 [hep-ph].
- [44] ALICE Collaboration, B. B. Abelev *et al.*, “Measurement of prompt D -meson production in $p - Pb$ collisions at $\sqrt{s_{NN}} = 5.02$ TeV,” *Phys. Rev. Lett.* **113** no. 23, (2014) 232301, arXiv:1405.3452 [nucl-ex].
- [45] J. Pumplin, D. R. Stump, J. Huston, H. L. Lai, P. M. Nadolsky, and W. K. Tung, “New generation of parton distributions with uncertainties from global QCD analysis,” *JHEP* **07** (2002) 012, arXiv:hep-ph/0201195 [hep-ph].
- [46] R. Gavin, Y. Li, F. Petriello, and S. Quackenbush, “FEWZ 2.0: A code for hadronic Z production at Next-to-Next-to-Leading order,” *Comput. Phys. Commun.* **182** (2011) 2388–2403, arXiv:1011.3540 [hep-ph].

- [47] A. D. Martin, W. J. Stirling, R. S. Thorne, and G. Watt, “Parton distributions for the LHC,” *Eur. Phys. J. C* **63** (2009) 189–285, [arXiv:0901.0002](https://arxiv.org/abs/0901.0002) [hep-ph].

A The ALICE Collaboration

J. Adam³⁹, D. Adamová⁸⁶, M.M. Aggarwal⁹⁰, G. Aglieri Rinella³⁵, M. Agnello^{113,31}, N. Agrawal⁴⁸, Z. Ahammed¹³⁷, S. Ahmad¹⁸, S.U. Ahn⁷⁰, S. Aiola¹⁴¹, A. Akindinov⁵⁵, S.N. Alam¹³⁷, D.S.D. Albuquerque¹²⁴, D. Aleksandrov⁸², B. Alessandro¹¹³, D. Alexandre¹⁰⁴, R. Alfaro Molina⁶⁵, A. Alici^{12,107}, A. Alkin³, J. Alme^{22,37}, T. Alt⁴², S. Altinpinar²², I. Altsybeev¹³⁶, C. Alves Garcia Prado¹²³, M. An⁷, C. Andrei⁸⁰, H.A. Andrews¹⁰⁴, A. Andronic¹⁰⁰, V. Anguelov⁹⁶, C. Anson⁸⁹, T. Antičić¹⁰¹, F. Antinori¹¹⁰, P. Antonioli¹⁰⁷, R. Anwar¹²⁶, L. Aphecetche¹¹⁶, H. Appelshäuser⁶¹, S. Arcelli²⁷, R. Arnaldi¹¹³, O.W. Arnold^{97,36}, I.C. Arsene²¹, M. Arslandok⁶¹, B. Audurier¹¹⁶, A. Augustinus³⁵, R. Averbek¹⁰⁰, M.D. Azmi¹⁸, A. Badalà¹⁰⁹, Y.W. Baek⁶⁹, S. Bagnasco¹¹³, R. Bailhache⁶¹, R. Bala⁹³, S. Balasubramanian¹⁴¹, A. Baldisseri¹⁵, R.C. Baral⁵⁸, A.M. Barbano²⁶, R. Barbera²⁸, F. Barile³³, G.G. Barnaföldi¹⁴⁰, L.S. Barnby^{35,104}, V. Barret⁷², P. Bartalini⁷, K. Barth³⁵, J. Bartke^{120,i}, E. Bartsch⁶¹, M. Basile²⁷, N. Bastid⁷², S. Basu¹³⁷, B. Bathen⁶², G. Batigne¹¹⁶, A. Batista Camejo⁷², B. Batyunya⁶⁸, P.C. Batzing²¹, I.G. Bearden⁸³, H. Beck⁹⁶, C. Bedda³¹, N.K. Behera⁵¹, I. Belikov⁶⁶, F. Bellini²⁷, H. Bello Martinez², R. Bellwied¹²⁶, L.G.E. Beltran¹²², V. Belyaev⁷⁷, G. Bencedi¹⁴⁰, S. Beole²⁶, A. Bercuci⁸⁰, Y. Berdnikov⁸⁸, D. Berenyi¹⁴⁰, R.A. Bertens^{54,129}, D. Berzano³⁵, L. Betev³⁵, A. Bhasin⁹³, I.R. Bhat⁹³, A.K. Bhati⁹⁰, B. Bhattacharjee⁴⁴, J. Bhom¹²⁰, L. Bianchi¹²⁶, N. Bianchi⁷⁴, C. Bianchin¹³⁹, J. Bielčák³⁹, J. Bielčiková⁸⁶, A. Bilandzic^{36,97}, G. Biro¹⁴⁰, R. Biswas⁴, S. Biswas^{81,4}, S. Bjelogrić⁵⁴, J.T. Blair¹²¹, D. Blau⁸², C. Blume⁶¹, F. Bock^{76,96}, A. Bogdanov⁷⁷, L. Boldizsár¹⁴⁰, M. Bombara⁴⁰, M. Bonora³⁵, J. Book⁶¹, H. Borel¹⁵, A. Borissov⁹⁹, M. Borri¹²⁸, F. Bossù⁶⁷, E. Botta²⁶, C. Bourjau⁸³, P. Braun-Munzinger¹⁰⁰, M. Bregant¹²³, T.A. Broker⁶¹, T.A. Browning⁹⁸, M. Broz³⁹, E.J. Brucken⁴⁶, E. Bruna¹¹³, G.E. Bruno³³, D. Budnikov¹⁰², H. Buesching⁶¹, S. Bufalino^{31,26}, P. Buhler¹¹⁵, S.A.I. Buitron⁶³, P. Buncic³⁵, O. Busch¹³², Z. Buthelezi⁶⁷, J.B. Butt¹⁶, J.T. Buxton¹⁹, J. Cabala¹¹⁸, D. Caffarri³⁵, H. Caines¹⁴¹, A. Caliva⁵⁴, E. Calvo Villar¹⁰⁵, P. Camerini²⁵, F. Carena³⁵, W. Carena³⁵, F. Carnesecchi^{12,27}, J. Castillo Castellanos¹⁵, A.J. Castro¹²⁹, E.A.R. Casula²⁴, C. Ceballos Sanchez⁹, J. Cepila³⁹, P. Cerello¹¹³, J. Cerkala¹¹⁸, B. Chang¹²⁷, S. Chapeland³⁵, M. Chartier¹²⁸, J.L. Charvet¹⁵, S. Chattopadhyay¹³⁷, S. Chattopadhyay¹⁰³, A. Chauvin^{97,36}, V. Chelnokov³, M. Cherney⁸⁹, C. Cheshkov¹³⁴, B. Cheynis¹³⁴, V. Chibante Barroso³⁵, D.D. Chinellato¹²⁴, S. Cho⁵¹, P. Chochula³⁵, K. Choi⁹⁹, M. Chojnacki⁸³, S. Choudhury¹³⁷, P. Christakoglou⁸⁴, C.H. Christensen⁸³, P. Christiansen³⁴, T. Chujo¹³², S.U. Chung⁹⁹, C. Cicalo¹⁰⁸, L. Cifarelli^{12,27}, F. Cindolo¹⁰⁷, J. Cleymans⁹², F. Colamaria³³, D. Colella^{56,35}, A. Collu⁷⁶, M. Colocci²⁷, G. Conesa Balbastre⁷³, Z. Conesa del Valle⁵², M.E. Connors^{141,ii}, J.G. Contreras³⁹, T.M. Cormier⁸⁷, Y. Corrales Morales¹¹³, I. Cortés Maldonado², P. Cortese³², M.R. Cosentino^{123,125}, F. Costa³⁵, J. Crkovská⁵², P. Crochet⁷², R. Cruz Albino¹¹, E. Cuautle⁶³, L. Cunqueiro^{35,62}, T. Dahms^{36,97}, A. Dainese¹¹⁰, M.C. Danisch⁹⁶, A. Danu⁵⁹, D. Das¹⁰³, I. Das¹⁰³, S. Das⁴, A. Dash⁸¹, S. Dash⁴⁸, S. De^{49,123}, A. De Caro³⁰, G. de Cataldo¹⁰⁶, C. de Conti¹²³, J. de Cuveland⁴², A. De Falco²⁴, D. De Gruttola^{30,12}, N. De Marco¹¹³, S. De Pasquale³⁰, R.D. De Souza¹²⁴, A. Deisting^{96,100}, A. Deloff⁷⁹, C. Deplano⁸⁴, P. Dhankher⁴⁸, D. Di Bari³³, A. Di Mauro³⁵, P. Di Nezza⁷⁴, B. Di Ruzza¹¹⁰, M.A. Diaz Corchero¹⁰, T. Dietel⁹², P. Dillenseger⁶¹, R. Divià³⁵, Ø. Djuvland²², A. Dobrin^{84,35}, D. Domenicis Gimenez¹²³, B. Dönigus⁶¹, O. Dordic²¹, T. Drozhzhova⁶¹, A.K. Dubey¹³⁷, A. Dubla¹⁰⁰, L. Ducroux¹³⁴, A.K. Duggal⁹⁰, P. Dupieux⁷², R.J. Ehlers¹⁴¹, D. Elia¹⁰⁶, E. Endress¹⁰⁵, H. Engel⁶⁰, E. Epple¹⁴¹, B. Erazmus¹¹⁶, F. Erhardt¹³³, B. Espagnon⁵², S. Esumi¹³², G. Eulisse³⁵, J. Eum⁹⁹, D. Evans¹⁰⁴, S. Evdokimov¹¹⁴, G. Eyyubova³⁹, L. Fabbietti^{36,97}, D. Fabris¹¹⁰, J. Faivre⁷³, A. Fantoni⁷⁴, M. Fasel^{87,76}, L. Feldkamp⁶², A. Feliciello¹¹³, G. Feofilov¹³⁶, J. Ferencei⁸⁶, A. Fernández Téllez², E.G. Ferreira¹⁷, A. Ferretti²⁹, V.J.G. Feuillard^{72,15}, J. Figiel¹²⁰, M.A.S. Figueredo¹²³, S. Filchagin¹⁰², D. Finogeev⁵³, F.M. Fionda²⁴, E.M. Fiore³³, M. Floris³⁵, S. Foertsch⁶⁷, P. Foka¹⁰⁰, S. Fokin⁸², E. Fragiaco¹¹², A. Francescon³⁵, A. Francisco¹¹⁶, U. Frankendorf¹⁰⁰, G.G. Fronze²⁶, U. Fuchs³⁵, C. Furget⁷³, A. Furs⁵³, M. Fusco Girard³⁰, J.J. Gaardhøje⁸³, M. Gagliardi²⁶, A.M. Gago¹⁰⁵, K. Gajdosova⁸³, M. Gallio²⁶, C.D. Galvan¹²², D.R. Gangadharan⁷⁶, P. Ganoti^{91,35}, C. Gao⁷, C. Garabatos¹⁰⁰, E. Garcia-Solis¹³, K. Garg²⁸, P. Garg⁴⁹, C. Gargiulo³⁵, P. Gasik^{97,36}, E.F. Gauger¹²¹, M.B. Gay Ducati⁶⁴, M. Germain¹¹⁶, P. Ghosh¹³⁷, S.K. Ghosh⁴, P. Gianotti⁷⁴, P. Giubellino^{113,35}, P. Giubilato²⁹, E. Gladysz-Dziadus¹²⁰, P. Glässel⁹⁶, D.M. Gómez Coral⁶⁵, A. Gomez Ramirez⁶⁰, A.S. Gonzalez³⁵, V. Gonzalez¹⁰, P. González-Zamora¹⁰, S. Gorbunov⁴², L. Görlich¹²⁰, S. Gotovac¹¹⁹, V. Grabski⁶⁵, L.K. Graczykowski¹³⁸, K.L. Graham¹⁰⁴, L. Greiner⁷⁶, A. Grelli⁵⁴, C. Grigoras³⁵, V. Grigoriev⁷⁷, A. Grigoryan¹, S. Grigoryan⁶⁸, N. Grion¹¹², J.M. Gronefeld¹⁰⁰, J.F. Grosse-Oetringhaus³⁵, R. Grosso¹⁰⁰, L. Gruber¹¹⁵, F. Guber⁵³, R. Guernane^{73,35}, B. Guerzoni²⁷, K. Gulbrandsen⁸³, T. Gunji¹³¹, A. Gupta⁹³, R. Gupta⁹³, I.B. Guzman², R. Haake^{35,62}, C. Hadjidakis⁵², H. Hamagaki^{131,78}, G. Hamar¹⁴⁰, J.C. Hamon⁶⁶, J.W. Harris¹⁴¹, A. Harton¹³, D. Hatzifotiadou¹⁰⁷, S. Hayashi¹³¹, S.T. Heckel⁶¹, E. Hellbär⁶¹, H. Helstrup³⁷, A. Herghelegiu⁸⁰, G. Herrera Corral¹¹, F. Herrmann⁶², B.A. Hess⁹⁵, K.F. Hetland³⁷, H. Hillemanns³⁵, B. Hippolyte⁶⁶, J. Hladky⁵⁷, D. Horak³⁹, R. Hosokawa¹³², P. Hristov³⁵, C. Hughes¹²⁹, T.J. Humanic¹⁹, N. Hussain⁴⁴, T. Hussain¹⁸, D. Hutter⁴², D.S. Hwang²⁰,

R. Ilkaev¹⁰², M. Inaba¹³², M. Ippolitov^{77,82}, M. Irfan¹⁸, V. Isakov⁵³, M.S. Islam⁴⁹, M. Ivanov^{35,100}, V. Ivanov⁸⁸, V. Izucheev¹¹⁴, B. Jacak⁷⁶, N. Jacazio²⁷, P.M. Jacobs⁷⁶, M.B. Jadhav⁴⁸, S. Jadlovská¹¹⁸, J. Jadlovsky¹¹⁸, C. Jahnke^{123,36}, M.J. Jakubowska¹³⁸, M.A. Janik¹³⁸, P.H.S.Y. Jayarathna¹²⁶, C. Jena⁸¹, S. Jena¹²⁶, R.T. Jimenez Bustamante¹⁰⁰, P.G. Jones¹⁰⁴, A. Jusko¹⁰⁴, P. Kalinak⁵⁶, A. Kalweit³⁵, J.H. Kang¹⁴², V. Kaplin⁷⁷, S. Kar¹³⁷, A. Karasu Uysal⁷¹, O. Karavichev⁵³, T. Karavicheva⁵³, L. Karayan^{100,96}, E. Karpechev⁵³, U. Kebschull⁶⁰, R. Keidel¹⁴³, D.L.D. Keijdener⁵⁴, M. Keil³⁵, M. Mohisin Khan^{18,iii}, P. Khan¹⁰³, S.A. Khan¹³⁷, A. Khanzadeev⁸⁸, Y. Kharlov¹¹⁴, A. Khatun¹⁸, A. Khuntia⁴⁹, B. Kileng³⁷, D.W. Kim⁴³, D.J. Kim¹²⁷, D. Kim¹⁴², H. Kim¹⁴², J.S. Kim⁴³, J. Kim⁹⁶, M. Kim⁵¹, M. Kim¹⁴², S. Kim²⁰, T. Kim¹⁴², S. Kirsch⁴², I. Kisel⁴², S. Kiselev⁵⁵, A. Kisiel¹³⁸, G. Kiss¹⁴⁰, J.L. Klay⁶, C. Klein⁶¹, J. Klein³⁵, C. Klein-Bösing⁶², S. Klewin⁹⁶, A. Kluge³⁵, M.L. Knichel⁹⁶, A.G. Knospe^{121,126}, C. Kobdaj¹¹⁷, M. Kofarago³⁵, T. Kollegger¹⁰⁰, A. Kolojvari¹³⁶, V. Kondratiev¹³⁶, N. Kondratyeva⁷⁷, E. Kondratyuk¹¹⁴, A. Konevskikh⁵³, M. Kopcik¹¹⁸, M. Kour⁹³, C. Kouzinopoulos³⁵, O. Kovalenko⁷⁹, V. Kovalenko¹³⁶, M. Kowalski¹²⁰, G. Koyithatta Meethalevedu⁴⁸, I. Králik⁵⁶, A. Kravčáková⁴⁰, M. Krivda^{104,56}, F. Krizek⁸⁶, E. Kryshen^{88,35}, M. Krzewicki⁴², A.M. Kubera¹⁹, V. Kučera⁸⁶, C. Kuhn⁶⁶, P.G. Kuijter⁸⁴, A. Kumar⁹³, J. Kumar⁴⁸, L. Kumar⁹⁰, S. Kumar⁴⁸, S. Kundu⁸¹, P. Kurashvili⁷⁹, A. Kurepin⁵³, A.B. Kurepin⁵³, A. Kuryakin¹⁰², S. Kushpil⁸⁶, M.J. Kweon⁵¹, Y. Kwon¹⁴², S.L. La Pointe⁴², P. La Rocca²⁸, C. Lagana Fernandes¹²³, I. Lakomov³⁵, R. Langoy⁴¹, K. Lapidus^{36,141}, C. Lara⁶⁰, A. Lardeux¹⁵, A. Lattuca²⁶, E. Laudi³⁵, L. Lazaridis³⁵, R. Lea²⁵, L. Leardini⁹⁶, S. Lee¹⁴², F. Lehas⁸⁴, S. Lehner¹¹⁵, J. Lehrbach⁴², R.C. Lemmon⁸⁵, V. Lenti¹⁰⁶, E. Leogrande⁵⁴, I. León Monzón¹²², P. Lévai¹⁴⁰, S. Li⁷, X. Li¹⁴, J. Lien⁴¹, R. Lietava¹⁰⁴, S. Lindal²¹, V. Lindenstruth⁴², C. Lippmann¹⁰⁰, M.A. Lisa¹⁹, H.M. Ljunggren³⁴, W. Llope¹³⁹, D.F. Lodato⁵⁴, P.I. Loenne²², V. Loginov⁷⁷, C. Loizides⁷⁶, X. Lopez⁷², E. López Torres⁹, A. Lowe¹⁴⁰, P. Luettig⁶¹, M. Lunardon²⁹, G. Luparello²⁵, M. Lupi³⁵, T.H. Lutz¹⁴¹, A. Maevskaya⁵³, M. Mager³⁵, S. Mahajan⁹³, S.M. Mahmood²¹, A. Maire⁶⁶, R.D. Majka¹⁴¹, M. Malaev⁸⁸, I. Maldonado Cervantes⁶³, L. Malinina^{68,iv}, D. Mal'Kevich⁵⁵, P. Malzacher¹⁰⁰, A. Mamonov¹⁰², V. Manko⁸², F. Manso⁷², V. Manzari¹⁰⁶, Y. Mao⁷, M. Marchisone^{67,130}, J. Mareš⁵⁷, G.V. Margagliotti²⁵, A. Margotti¹⁰⁷, J. Margutti⁵⁴, A. Marín¹⁰⁰, C. Markert¹²¹, M. Marquard⁶¹, N.A. Martin¹⁰⁰, P. Martinengo³⁵, M.I. Martínez², G. Martínez García¹¹⁶, M. Martinez Pedreira³⁵, A. Mas¹²³, S. Masciocchi¹⁰⁰, M. Maserà²⁶, A. Masoni¹⁰⁸, A. Mastroserio³³, A.M. Mathis^{36,97}, A. Matyja^{129,120}, C. Mayer¹²⁰, J. Mazer¹²⁹, M. Mazzilli³³, M.A. Mazzoni¹¹¹, F. Meddi²³, Y. Melikyan⁷⁷, A. Menchaca-Rocha⁶⁵, E. Meninno³⁰, J. Mercado Pérez⁹⁶, M. Meres³⁸, S. Mhlanga⁹², Y. Miake¹³², M.M. Mieskolainen⁴⁶, K. Mikhaylov^{55,68}, L. Milano⁷⁶, J. Milosevic²¹, A. Mischke⁵⁴, A.N. Mishra⁴⁹, T. Mishra⁵⁸, D. Miśkowiec¹⁰⁰, J. Mitra¹³⁷, C.M. Miti⁵⁹, N. Mohammadi⁵⁴, B. Mohanty⁸¹, L. Molnar¹¹⁶, E. Montes¹⁰, D.A. Moreira De Godoy⁶², L.A.P. Moreno², S. Moretto²⁹, A. Morreale¹¹⁶, A. Morsch³⁵, V. Muccifora⁷⁴, E. Mudnic¹¹⁹, D. Mühlheim⁶², S. Muhuri¹³⁷, M. Mukherjee¹³⁷, J.D. Mulligan¹⁴¹, M.G. Munhoz¹²³, K. Münnig⁴⁵, R.H. Munzer^{36,61,97}, H. Murakami¹³¹, S. Murray⁶⁷, L. Musa³⁵, J. Musinsky⁵⁶, C.J. Myers¹²⁶, B. Naik⁴⁸, R. Nair⁷⁹, B.K. Nandi⁴⁸, R. Nania¹⁰⁷, E. Nappi¹⁰⁶, M.U. Naru¹⁶, H. Natal da Luz¹²³, C. Nattrass¹²⁹, S.R. Navarro², K. Nayak⁸¹, R. Nayak⁴⁸, T.K. Nayak¹³⁷, S. Nazarenko¹⁰², A. Nedosekin⁵⁵, R.A. Negrao De Oliveira³⁵, L. Nellen⁶³, F. Ng¹²⁶, M. Nicassio¹⁰⁰, M. Niculescu⁵⁹, J. Niedziela³⁵, B.S. Nielsen⁸³, S. Nikolaev⁸², S. Nikulin⁸², V. Nikulin⁸⁸, F. Noferini^{12,107}, P. Nomokonov⁶⁸, G. Nooren⁵⁴, J.C.C. Noris², J. Norman¹²⁸, A. Nyanin⁸², J. Nystrand²², H. Oeschler⁹⁶, S. Oh¹⁴¹, A. Ohlson³⁵, T. Okubo⁴⁷, L. Olah¹⁴⁰, J. Oleniacz¹³⁸, A.C. Oliveira Da Silva¹²³, M.H. Oliver¹⁴¹, J. Onderwaater¹⁰⁰, C. Oppedisano¹¹³, R. Orava⁴⁶, M. Oravec¹¹⁸, A. Ortiz Velasquez⁶³, A. Oskarsson³⁴, J. Otwinowski¹²⁰, K. Oyama⁷⁸, M. Ozdemir⁶¹, Y. Pachmayer⁹⁶, V. Pacik⁸³, D. Pagano^{135,26}, P. Pagano³⁰, G. Paic⁶³, S.K. Pal¹³⁷, P. Palni⁷, J. Pan¹³⁹, A.K. Pandey⁴⁸, V. Papikyan¹, G.S. Pappalardo¹⁰⁹, P. Pareek⁴⁹, J. Park⁵¹, W.J. Park¹⁰⁰, S. Parmar⁹⁰, A. Passfeld⁶², V. Paticchio¹⁰⁶, R.N. Patra¹³⁷, B. Paul¹¹³, H. Pei⁷, T. Peitzmann⁵⁴, X. Peng⁷, H. Pereira Da Costa¹⁵, D. Peresunko^{77,82}, E. Perez Lezama⁶¹, V. Peskov⁶¹, Y. Pestov⁵, V. Petráček³⁹, V. Petrov¹¹⁴, M. Petrovici⁸⁰, C. Petta²⁸, S. Piano¹¹², M. Pikna³⁸, P. Pillot¹¹⁶, L.O.D.L. Pimentel⁸³, O. Pinazza^{35,107}, L. Pinsky¹²⁶, D.B. Piyarathna¹²⁶, M. Płoskoń⁷⁶, M. Planinic¹³³, J. Pluta¹³⁸, S. Pochybova¹⁴⁰, P.L.M. Podesta-Lerma¹²², M.G. Poghosyan⁸⁷, B. Polichtchouk¹¹⁴, N. Poljak¹³³, W. Poonsawat¹¹⁷, A. Pop⁸⁰, H. Poppenborg⁶², S. Porteboeuf-Houssais⁷², J. Porter⁷⁶, J. Pospisil⁸⁶, V. Pozdniakov⁶⁸, S.K. Prasad⁴, R. Preghenella^{107,35}, F. Prino¹¹³, C.A. Pruneau¹³⁹, I. Pshenichnov⁵³, M. Puccio²⁶, G. Puddu²⁴, P. Pujahari¹³⁹, V. Punin¹⁰², J. Putschke¹³⁹, H. Qvigstad²¹, A. Rachevski¹¹², S. Raha⁴, S. Rajput⁹³, J. Rak¹²⁷, A. Rakotozafindrabe¹⁵, L. Ramello³², F. Rami⁶⁶, D.B. Rana¹²⁶, R. Raniwala⁹⁴, S. Raniwala⁹⁴, S.S. Räsänen⁴⁶, B.T. Rascanu⁶¹, D. Rathee⁹⁰, V. Ratza⁴⁵, I. Ravasenga²⁶, K.F. Read^{87,129}, K. Redlich⁷⁹, A. Rehman²², P. Reichelt⁶¹, F. Reidt^{35,96}, X. Ren⁷, R. Renfordt⁶¹, A.R. Reolon⁷⁴, A. Reshetin⁵³, K. Reygers⁹⁶, V. Riabov⁸⁸, R.A. Ricci⁷⁵, T. Richert^{34,54}, M. Richter²¹, P. Riedler³⁵, W. Riegler³⁵, F. Riggi²⁸, C. Ristea⁵⁹, M. Rodríguez Cahuantzi², K. Røed²¹, E. Rogochaya⁶⁸, D. Rohr⁴², D. Röhrich²², F. Ronchetti^{35,74}, L. Ronflette¹¹⁶, P. Rosnet⁷², A. Rossi²⁹, F. Roukoutakis⁹¹, A. Roy⁴⁹, C. Roy⁶⁶, P. Roy¹⁰³, A.J. Rubio Montero¹⁰,

R. Rui²⁵, R. Russo²⁶, E. Ryabinkin⁸², Y. Ryabov⁸⁸, A. Rybicki¹²⁰, S. Saarinen⁴⁶, S. Sadhu¹³⁷, S. Sadovsky¹¹⁴, K. Šafařík³⁵, B. Sahlmuller⁶¹, B. Sahoo⁴⁸, P. Sahoo⁴⁹, R. Sahoo⁴⁹, S. Sahoo⁵⁸, P.K. Sahu⁵⁸, J. Saini¹³⁷, S. Sakai^{132,74}, M.A. Saleh¹³⁹, J. Salzwedel¹⁹, S. Sambyal⁹³, V. Samsonov^{77,88}, A. Sandoval⁶⁵, M. Sano¹³², D. Sarkar¹³⁷, N. Sarkar¹³⁷, P. Sarma⁴⁴, M.H.P. Sas⁵⁴, E. Scapparone¹⁰⁷, F. Scarlassara²⁹, R.P. Scharenberg⁹⁸, C. Schiaua⁸⁰, R. Schicker⁹⁶, C. Schmidt¹⁰⁰, H.R. Schmidt⁹⁵, M. Schmidt⁹⁵, J. Schukraft³⁵, Y. Schutz^{116,35,66}, K. Schwarz¹⁰⁰, K. Schweda¹⁰⁰, G. Scioli²⁷, E. Scomparin¹¹³, R. Scott¹²⁹, M. Šefčík⁴⁰, J.E. Seger⁸⁹, Y. Sekiguchi¹³¹, D. Sekihata⁴⁷, I. Selyuzhenkov¹⁰⁰, K. Senosi⁶⁷, S. Senyukov^{3,35}, E. Serradilla^{65,10}, P. Sett⁴⁸, A. Sevcenco⁵⁹, A. Shabanov⁵³, A. Shabetai¹¹⁶, O. Shadura³, R. Shahoyan³⁵, A. Shangaraev¹¹⁴, A. Sharma⁹³, A. Sharma⁹⁰, M. Sharma⁹³, M. Sharma⁹³, N. Sharma^{90,129}, A.I. Sheikh¹³⁷, K. Shigaki⁴⁷, Q. Shou⁷, K. Shtejer^{9,26}, Y. Sibiriyak⁸², S. Siddhanta¹⁰⁸, K.M. Sielewicz³⁵, T. Siemiarzczuk⁷⁹, D. Silvermyr³⁴, C. Silvestre⁷³, G. Simatovic¹³³, G. Simonetti³⁵, R. Singaravelu¹³⁷, R. Singh⁸¹, V. Singhal¹³⁷, T. Sinha¹⁰³, B. Sitar³⁸, M. Sitta³², T.B. Skaali²¹, M. Slupecki¹²⁷, N. Smirnov¹⁴¹, R.J.M. Snellings⁵⁴, T.W. Snellman¹²⁷, J. Song⁹⁹, M. Song¹⁴², Z. Song⁷, F. Soramel²⁹, S. Sorensen¹²⁹, F. Sozzi¹⁰⁰, E. Spiriti⁷⁴, I. Sputowska¹²⁰, B.K. Srivastava⁹⁸, J. Stachel⁹⁶, I. Stan⁵⁹, P. Stankus⁸⁷, E. Stenlund³⁴, G. Steyn⁶⁷, J.H. Stiller⁹⁶, D. Stocco¹¹⁶, P. Strmen³⁸, A.A.P. Suaide¹²³, T. Sugitate⁴⁷, C. Suire⁵², M. Suleymanov¹⁶, M. Suljic²⁵, R. Sultanov⁵⁵, M. Šumbera⁸⁶, S. Sumowidagdo⁵⁰, K. Suzuki¹¹⁵, S. Swain⁵⁸, A. Szabo³⁸, I. Szarka³⁸, A. Szczepankiewicz¹³⁸, M. Szymanski¹³⁸, U. Tabassam¹⁶, J. Takahashi¹²⁴, G.J. Tambave²², N. Tanaka¹³², M. Tarhini⁵², M. Tariq¹⁸, M.G. Tarzila⁸⁰, A. Tauro³⁵, G. Tejada Muñoz², A. Telesca³⁵, K. Terasaki¹³¹, C. Terrevoli²⁹, B. Teyssier¹³⁴, D. Thakur⁴⁹, D. Thomas¹²¹, R. Tieulent¹³⁴, A. Tikhonov⁵³, A.R. Timmins¹²⁶, A. Toia⁶¹, S. Tripathy⁴⁹, S. Trogolo²⁶, G. Trombetta³³, V. Trubnikov³, W.H. Trzaska¹²⁷, T. Tsuji¹³¹, A. Tumkin¹⁰², R. Turrisi¹¹⁰, T.S. Tveter²¹, K. Ullaland²², E.N. Umaka¹²⁶, A. Uras¹³⁴, G.L. Usai²⁴, A. Utrobicic¹³³, M. Vala⁵⁶, J. Van Der Maarel⁵⁴, J.W. Van Hoorne³⁵, M. van Leeuwen⁵⁴, T. Vanat⁸⁶, P. Vande Vyvre³⁵, D. Varga¹⁴⁰, A. Vargas², M. Vargyas¹²⁷, R. Varma⁴⁸, M. Vasileiou⁹¹, A. Vasiliev⁸², A. Vauthier⁷³, O. Vázquez Doce^{36,97}, V. Vechernin¹³⁶, A.M. Veen⁵⁴, A. Velure²², E. Vercellin²⁶, S. Vergara Limón², R. Vernet⁸, R. Vértesi¹⁴⁰, L. Vickovic¹¹⁹, S. Vigolo⁵⁴, J. Viinikainen¹²⁷, Z. Vilakazi¹³⁰, O. Villalobos Baillie¹⁰⁴, A. Villatoro Tello², A. Vinogradov⁸², L. Vinogradov¹³⁶, T. Virgili³⁰, V. Vislavicius³⁴, A. Vodopyanov⁶⁸, M.A. Völkl⁹⁶, K. Voloshin⁵⁵, S.A. Voloshin¹³⁹, G. Volpe^{140,33}, B. von Haller³⁵, I. Vorobyev^{36,97}, D. Voscek¹¹⁸, D. Vranic^{35,100}, J. Vrláková⁴⁰, B. Wagner²², J. Wagner¹⁰⁰, H. Wang⁵⁴, M. Wang⁷, D. Watanabe¹³², Y. Watanabe¹³¹, M. Weber¹¹⁵, S.G. Weber¹⁰⁰, D.F. Weiser⁹⁶, J.P. Wessels⁶², U. Westerhoff⁶², A.M. Whitehead⁹², J. Wiechula⁶¹, J. Wikne²¹, G. Wilk⁷⁹, J. Wilkinson⁹⁶, G.A. Willems⁶², M.C.S. Williams¹⁰⁷, B. Windelband⁹⁶, M. Winn⁹⁶, W.E. Witt¹²⁹, S. Yalcin⁷¹, P. Yang⁷, S. Yano⁴⁷, Z. Yin⁷, H. Yokoyama^{132,73}, I.-K. Yoo^{35,99}, J.H. Yoon⁵¹, V. Yurchenko³, V. Zaccaro⁸³, A. Zaman¹⁶, C. Zampolli^{35,107}, H.J.C. Zanoli¹²³, S. Zaporozhets⁶⁸, N. Zardoshti¹⁰⁴, A. Zarochentsev¹³⁶, P. Závada⁵⁷, N. Zaviyalov¹⁰², H. Zbroszczyk¹³⁸, M. Zhalov⁸⁸, H. Zhang^{7,22}, X. Zhang^{76,7}, Y. Zhang⁷, C. Zhang⁵⁴, Z. Zhang⁷, C. Zhao²¹, N. Zhigareva⁵⁵, D. Zhou⁷, Y. Zhou⁸³, Z. Zhou²², H. Zhu^{7,22}, J. Zhu^{116,7}, A. Zichichi^{12,27}, A. Zimmermann⁹⁶, M.B. Zimmermann^{62,35}, G. Zinovjev³, J. Zmeskal¹¹⁵

Affiliation notes

- ⁱ Deceased
- ⁱⁱ Also at: Georgia State University, Atlanta, Georgia, United States
- ⁱⁱⁱ Also at: Also at Department of Applied Physics, Aligarh Muslim University, Aligarh, India
- ^{iv} Also at: M.V. Lomonosov Moscow State University, D.V. Skobeltsyn Institute of Nuclear, Physics, Moscow, Russia

Collaboration Institutes

- ¹A.I. Alikhanyan National Science Laboratory (Yerevan Physics Institute) Foundation, Yerevan, Armenia
- ²Benemérita Universidad Autónoma de Puebla, Puebla, Mexico
- ³Bogolyubov Institute for Theoretical Physics, Kiev, Ukraine
- ⁴Bose Institute, Department of Physics and Centre for Astroparticle Physics and Space Science (CAPSS), Kolkata, India
- ⁵Budker Institute for Nuclear Physics, Novosibirsk, Russia
- ⁶California Polytechnic State University, San Luis Obispo, California, United States
- ⁷Central China Normal University, Wuhan, China
- ⁸Centre de Calcul de l'IN2P3, Villeurbanne, Lyon, France
- ⁹Centro de Aplicaciones Tecnológicas y Desarrollo Nuclear (CEADEN), Havana, Cuba

- ¹⁰Centro de Investigaciones Energéticas Medioambientales y Tecnológicas (CIEMAT), Madrid, Spain
- ¹¹Centro de Investigación y de Estudios Avanzados (CINVESTAV), Mexico City and Mérida, Mexico
- ¹²Centro Fermi - Museo Storico della Fisica e Centro Studi e Ricerche “Enrico Fermi”, Rome, Italy
- ¹³Chicago State University, Chicago, Illinois, United States
- ¹⁴China Institute of Atomic Energy, Beijing, China
- ¹⁵Commissariat à l’Energie Atomique, IRFU, Saclay, France
- ¹⁶COMSATS Institute of Information Technology (CIIT), Islamabad, Pakistan
- ¹⁷Departamento de Física de Partículas and IGFAE, Universidad de Santiago de Compostela, Santiago de Compostela, Spain
- ¹⁸Department of Physics, Aligarh Muslim University, Aligarh, India
- ¹⁹Department of Physics, Ohio State University, Columbus, Ohio, United States
- ²⁰Department of Physics, Sejong University, Seoul, South Korea
- ²¹Department of Physics, University of Oslo, Oslo, Norway
- ²²Department of Physics and Technology, University of Bergen, Bergen, Norway
- ²³Dipartimento di Fisica dell’Università ‘La Sapienza’ and Sezione INFN, Rome, Italy
- ²⁴Dipartimento di Fisica dell’Università and Sezione INFN, Cagliari, Italy
- ²⁵Dipartimento di Fisica dell’Università and Sezione INFN, Trieste, Italy
- ²⁶Dipartimento di Fisica dell’Università and Sezione INFN, Turin, Italy
- ²⁷Dipartimento di Fisica e Astronomia dell’Università and Sezione INFN, Bologna, Italy
- ²⁸Dipartimento di Fisica e Astronomia dell’Università and Sezione INFN, Catania, Italy
- ²⁹Dipartimento di Fisica e Astronomia dell’Università and Sezione INFN, Padova, Italy
- ³⁰Dipartimento di Fisica ‘E.R. Caianiello’ dell’Università and Gruppo Collegato INFN, Salerno, Italy
- ³¹Dipartimento DISAT del Politecnico and Sezione INFN, Turin, Italy
- ³²Dipartimento di Scienze e Innovazione Tecnologica dell’Università del Piemonte Orientale and INFN Sezione di Torino, Alessandria, Italy
- ³³Dipartimento Interateneo di Fisica ‘M. Merlin’ and Sezione INFN, Bari, Italy
- ³⁴Division of Experimental High Energy Physics, University of Lund, Lund, Sweden
- ³⁵European Organization for Nuclear Research (CERN), Geneva, Switzerland
- ³⁶Excellence Cluster Universe, Technische Universität München, Munich, Germany
- ³⁷Faculty of Engineering, Bergen University College, Bergen, Norway
- ³⁸Faculty of Mathematics, Physics and Informatics, Comenius University, Bratislava, Slovakia
- ³⁹Faculty of Nuclear Sciences and Physical Engineering, Czech Technical University in Prague, Prague, Czech Republic
- ⁴⁰Faculty of Science, P.J. Šafárik University, Košice, Slovakia
- ⁴¹Faculty of Technology, Buskerud and Vestfold University College, Tonsberg, Norway
- ⁴²Frankfurt Institute for Advanced Studies, Johann Wolfgang Goethe-Universität Frankfurt, Frankfurt, Germany
- ⁴³Gangneung-Wonju National University, Gangneung, South Korea
- ⁴⁴Gauhati University, Department of Physics, Guwahati, India
- ⁴⁵Helmholtz-Institut für Strahlen- und Kernphysik, Rheinische Friedrich-Wilhelms-Universität Bonn, Bonn, Germany
- ⁴⁶Helsinki Institute of Physics (HIP), Helsinki, Finland
- ⁴⁷Hiroshima University, Hiroshima, Japan
- ⁴⁸Indian Institute of Technology Bombay (IIT), Mumbai, India
- ⁴⁹Indian Institute of Technology Indore, Indore, India
- ⁵⁰Indonesian Institute of Sciences, Jakarta, Indonesia
- ⁵¹Inha University, Incheon, South Korea
- ⁵²Institut de Physique Nucléaire d’Orsay (IPNO), Université Paris-Sud, CNRS-IN2P3, Orsay, France
- ⁵³Institute for Nuclear Research, Academy of Sciences, Moscow, Russia
- ⁵⁴Institute for Subatomic Physics of Utrecht University, Utrecht, Netherlands
- ⁵⁵Institute for Theoretical and Experimental Physics, Moscow, Russia
- ⁵⁶Institute of Experimental Physics, Slovak Academy of Sciences, Košice, Slovakia
- ⁵⁷Institute of Physics, Academy of Sciences of the Czech Republic, Prague, Czech Republic
- ⁵⁸Institute of Physics, Bhubaneswar, India
- ⁵⁹Institute of Space Science (ISS), Bucharest, Romania
- ⁶⁰Institut für Informatik, Johann Wolfgang Goethe-Universität Frankfurt, Frankfurt, Germany
- ⁶¹Institut für Kernphysik, Johann Wolfgang Goethe-Universität Frankfurt, Frankfurt, Germany

- ⁶²Institut für Kernphysik, Westfälische Wilhelms-Universität Münster, Münster, Germany
⁶³Instituto de Ciencias Nucleares, Universidad Nacional Autónoma de México, Mexico City, Mexico
⁶⁴Instituto de Física, Universidade Federal do Rio Grande do Sul (UFRGS), Porto Alegre, Brazil
⁶⁵Instituto de Física, Universidad Nacional Autónoma de México, Mexico City, Mexico
⁶⁶Institut Pluridisciplinaire Hubert Curien (IPHC), Université de Strasbourg, CNRS-IN2P3, Strasbourg, France
⁶⁷iThemba LABS, National Research Foundation, Somerset West, South Africa
⁶⁸Joint Institute for Nuclear Research (JINR), Dubna, Russia
⁶⁹Konkuk University, Seoul, South Korea
⁷⁰Korea Institute of Science and Technology Information, Daejeon, South Korea
⁷¹KTO Karatay University, Konya, Turkey
⁷²Laboratoire de Physique Corpusculaire (LPC), Clermont Université, Université Blaise Pascal, CNRS-IN2P3, Clermont-Ferrand, France
⁷³Laboratoire de Physique Subatomique et de Cosmologie, Université Grenoble-Alpes, CNRS-IN2P3, Grenoble, France
⁷⁴Laboratori Nazionali di Frascati, INFN, Frascati, Italy
⁷⁵Laboratori Nazionali di Legnaro, INFN, Legnaro, Italy
⁷⁶Lawrence Berkeley National Laboratory, Berkeley, California, United States
⁷⁷Moscow Engineering Physics Institute, Moscow, Russia
⁷⁸Nagasaki Institute of Applied Science, Nagasaki, Japan
⁷⁹National Centre for Nuclear Studies, Warsaw, Poland
⁸⁰National Institute for Physics and Nuclear Engineering, Bucharest, Romania
⁸¹National Institute of Science Education and Research, Bhubaneswar, India
⁸²National Research Centre Kurchatov Institute, Moscow, Russia
⁸³Niels Bohr Institute, University of Copenhagen, Copenhagen, Denmark
⁸⁴Nikhef, Nationaal instituut voor subatomaire fysica, Amsterdam, Netherlands
⁸⁵Nuclear Physics Group, STFC Daresbury Laboratory, Daresbury, United Kingdom
⁸⁶Nuclear Physics Institute, Academy of Sciences of the Czech Republic, Řež u Prahy, Czech Republic
⁸⁷Oak Ridge National Laboratory, Oak Ridge, Tennessee, United States
⁸⁸Petersburg Nuclear Physics Institute, Gatchina, Russia
⁸⁹Physics Department, Creighton University, Omaha, Nebraska, United States
⁹⁰Physics Department, Panjab University, Chandigarh, India
⁹¹Physics Department, University of Athens, Athens, Greece
⁹²Physics Department, University of Cape Town, Cape Town, South Africa
⁹³Physics Department, University of Jammu, Jammu, India
⁹⁴Physics Department, University of Rajasthan, Jaipur, India
⁹⁵Physikalisches Institut, Eberhard Karls Universität Tübingen, Tübingen, Germany
⁹⁶Physikalisches Institut, Ruprecht-Karls-Universität Heidelberg, Heidelberg, Germany
⁹⁷Physik Department, Technische Universität München, Munich, Germany
⁹⁸Purdue University, West Lafayette, Indiana, United States
⁹⁹Pusan National University, Pusan, South Korea
¹⁰⁰Research Division and ExtreMe Matter Institute EMMI, GSI Helmholtzzentrum für Schwerionenforschung, Darmstadt, Germany
¹⁰¹Rudjer Bošković Institute, Zagreb, Croatia
¹⁰²Russian Federal Nuclear Center (VNIIEF), Sarov, Russia
¹⁰³Saha Institute of Nuclear Physics, Kolkata, India
¹⁰⁴School of Physics and Astronomy, University of Birmingham, Birmingham, United Kingdom
¹⁰⁵Sección Física, Departamento de Ciencias, Pontificia Universidad Católica del Perú, Lima, Peru
¹⁰⁶Sezione INFN, Bari, Italy
¹⁰⁷Sezione INFN, Bologna, Italy
¹⁰⁸Sezione INFN, Cagliari, Italy
¹⁰⁹Sezione INFN, Catania, Italy
¹¹⁰Sezione INFN, Padova, Italy
¹¹¹Sezione INFN, Rome, Italy
¹¹²Sezione INFN, Trieste, Italy
¹¹³Sezione INFN, Turin, Italy
¹¹⁴SSC IHEP of NRC Kurchatov institute, Protvino, Russia

- ¹¹⁵Stefan Meyer Institut für Subatomare Physik (SMI), Vienna, Austria
¹¹⁶SUBATECH, Ecole des Mines de Nantes, Université de Nantes, CNRS-IN2P3, Nantes, France
¹¹⁷Suranaree University of Technology, Nakhon Ratchasima, Thailand
¹¹⁸Technical University of Košice, Košice, Slovakia
¹¹⁹Technical University of Split FESB, Split, Croatia
¹²⁰The Henryk Niewodniczanski Institute of Nuclear Physics, Polish Academy of Sciences, Cracow, Poland
¹²¹The University of Texas at Austin, Physics Department, Austin, Texas, United States
¹²²Universidad Autónoma de Sinaloa, Culiacán, Mexico
¹²³Universidade de São Paulo (USP), São Paulo, Brazil
¹²⁴Universidade Estadual de Campinas (UNICAMP), Campinas, Brazil
¹²⁵Universidade Federal do ABC, Santo Andre, Brazil
¹²⁶University of Houston, Houston, Texas, United States
¹²⁷University of Jyväskylä, Jyväskylä, Finland
¹²⁸University of Liverpool, Liverpool, United Kingdom
¹²⁹University of Tennessee, Knoxville, Tennessee, United States
¹³⁰University of the Witwatersrand, Johannesburg, South Africa
¹³¹University of Tokyo, Tokyo, Japan
¹³²University of Tsukuba, Tsukuba, Japan
¹³³University of Zagreb, Zagreb, Croatia
¹³⁴Université de Lyon, Université Lyon 1, CNRS/IN2P3, IPN-Lyon, Villeurbanne, Lyon, France
¹³⁵Università di Brescia, Brescia, Italy
¹³⁶V. Fock Institute for Physics, St. Petersburg State University, St. Petersburg, Russia
¹³⁷Variable Energy Cyclotron Centre, Kolkata, India
¹³⁸Warsaw University of Technology, Warsaw, Poland
¹³⁹Wayne State University, Detroit, Michigan, United States
¹⁴⁰Wigner Research Centre for Physics, Hungarian Academy of Sciences, Budapest, Hungary
¹⁴¹Yale University, New Haven, Connecticut, United States
¹⁴²Yonsei University, Seoul, South Korea
¹⁴³Zentrum für Technologietransfer und Telekommunikation (ZTT), Fachhochschule Worms, Worms, Germany